Chem Soc Rev

Black titanium dioxide (TiO2) nanomaterials

Journal:	*Chemical Society Reviews*
Manuscript ID:	CS-CRV-09-2014-000330.R2
Article Type:	Review Article
Date Submitted by the Author:	30-Sep-2014
Complete List of Authors:	Chen, Xiaobo; University of Missouri - Kansas City, Department of Chemistry liu, lei; Changchun Institute of Optics, Fine Mechanics and Physics, Chinese Academy of Sciences, Huang, Fu Qiang; Shanghai Institute of Ceramics, State Key Laboratory of High Performance Ceramics and Superfine Microstructures

Black titanium dioxide (TiO_2) nanomaterials

Xiaobo Chen,[1,*] Lei Liu,[2] Fuqiang Huang[3]

1. Department of Chemistry, University of Missouri – Kansas City, Kansas City, MO 64110, U.S.A.

2. State Key Laboratory of Luminescence and Applications, Changchun Institute of Optics, Fine Mechanics and Physics, Chinese Academy of Sciences, 130033, Changchun, Jilin, P. R. China.

3. Beijing National Laboratory for Molecular Sciences and State Key Laboratory of Rare Earth Materials Chemistry and Applications, College of Chemistry and Molecular Engineering, Peking University, Beijing 100871, P. R. China; Shanghai Institute of Ceramics, State Key Laboratory of High Performance Ceramics and Superfine Microstructures, Shanghai 200050, P. R. China.

Corresponding Author:

Xiaobo Chen

Email: chenxiaobo@umkc.edu

TOC:

Abstract

In the past decades, there has been a wide research interest on titanium dioxide (TiO_2) nanomaterials due to their applications in photocatalytic hydrogen generation and environmental pollution removal. Improving the optical absorption properties of TiO_2 nanomaterials has been successfully demonstrated to enhance their photocatalytic activities, especially in the report of black TiO_2 nanoparticles. The recent progress in the investigation of black TiO_2 nanomaterials has been reviewed here, and special emphasis has been given on their fabrication methods along with their various chemical/physical properties and applications.

1. Introduction

TiO_2 nanomaterials have attracted tremendous interest due to their main applications in photocatalytic hydrogen generation and environmental pollution removal.[1-10] There are three main crystal phases for TiO_2: anatase, rutile and brookite,[9] and many other minor phases such as monoclinic TiO_2 (B).[10-12] All of them have large electronic bandgaps of 3.0 – 3.2 eV.[9-14] This limits their optical absorption in the ultraviolet (UV) region of the solar spectrum. This part, however, only accounts for less than 5% of the entire solar energy.[15] Even if TiO_2 is very efficient in utilizing the UV light, its overall solar activity is thus very limited. The photocatalytic activity depends on the amount of working electrons and holes on the surface of the photocatalyst for the reaction. In the photocatalytic process, TiO_2 absorbs light with energy larger than its bandgap and produces excited electrons in the conduction band and excited holes in the valence band.[7,14] These excited charges may separate from each other and migrate to its surface to perform photocatalytic reactions. During the charge separation and migration processes, some of the excited charges may recombine and disappear. Nevertheless, the amount of excited charges on the surface is generated from the absorption process. The more light TiO_2 can absorb, the more excited charges are likely to be on the surface. Therefore, it has become a common sense to improve the optical absorption properties of TiO_2 in order to enhance its overall activity.

During the past decades, much effort has been devoted to make TiO_2 colorful for better optical absorption through metal or non-metal doping. For examples, a series of metal ions have been used to replace the Ti^{4+} ions in the TiO_2 lattice to bring about visible-light absorption since early 1990s,[16-39] non-metal elements have been adopted to

replace the O^{2-} ions in the TiO_2 lattice since 2001,[40-66] and metal and non-metal elements has been combined to replace partial Ti^{4+} and O^{2-} ions in the TiO_2 lattice recently.[67-74] All these efforts have brought about the absorption of TiO_2 into the visible-light region and improved photocatalytic activity has been frequently reported.

Thermodynamically the water splitting potential is only 1.23 V. So in the ideal case for photocatalytic water splitting, the bandgap of semiconductor should be around 1.23 eV, assuming that the overpotentials for the oxygen and hydrogen evolutions are successfully removed and the electronic structures of the semiconductor align perfectly with the water redox potentials. This bandgap corresponds to 1000 nm in wavelength. So, ideally, the color of TiO_2 should be tuned to black, with energy gap of 1.23 eV and optical absorption near 1000 nm in the near infrared region. In 2011, hydrogenation has been reported as an effective approach in shifting the bandgap of TiO_2 to around 1.5 eV with optical onset around 1.0 eV and color of black.[75] Unsurprisingly, this discovery has triggered world-wide research interest on black TiO_2 nanomaterials.[76-78] Indeed, it is well known that heating TiO_2 under vacuum or in a reducing atmosphere leads to color changes.[6] Ti^{3+} or/and oxygen vacancies turn white TiO_2 into yellow, blue or black material.[6]

Here we would like to summarize the recent research progress on the black TiO_2 nanomaterials. Specifically, in this review, we focus on the formation of black TiO_2 nanoparticles. Traditional reduction treatments of TiO_2 bulk crystals or surfaces and those led to apparent phase transformations are not reviewed here. If a material absorbs 100% light across the whole visible-light, it shows a completely black color. If only certain percentage across the entire visible-light region is equally absorbs, it is partially black or

gray. If no light is absorbed across the entire visible-light region, the color is white. If the light across the entire visible-light region is not equally absorbed, certain color (e.g., yellow, brown, green) will be observed. In this review, we focus only on the recent synthesis of black or partially black TiO_2 nanomaterials, especially on their detailed synthetic conditions, as these conditions strongly affect the properties and performance of the obtained TiO_2 nanomaterials. Those studies introducing other elements into the lattice or surface of TiO_2 to obtain black color will not be reviewed. Then we briefly summarize their chemical and structural properties and various applications. Although the change in optical absorption properties is the one main reason for the enhanced photocatalytic activities, however, this does not mean that the color change plays the same role for all applications, such as in batteries, supercapacitors, and catalytic reaction of ethylene to polyethylene (new application of TiO_2 nanoparticles). Nevertheless, we hope this review will inspire more advance in this area in the future.

2. Synthesis of black TiO_2 nanomaterials

2.1 Hydrogen thermal treatment

Intuition tells us that hydrogen thermal treatment of TiO_2 nanocrystals is simple and straightforward as hydrogen will reduce TiO_2 into other chemical species where Ti^{4+} should become Ti^{3+} or other reduction states, and their lattice structure and other physical/chemical properties change accordingly. However, this reaction seems not as simple as we thought.

$$TiO_2 + xH_2 \xrightarrow{\Delta} TiO_2, TiO_{2-x}, TiO_{2-x}H_{2x}...? \quad (1)$$

As seem from this reaction scheme (1), the amount of reactants, the chemical properties of the starting TiO_2 nanomaterials, the pressure and concentration of the hydrogen gas, the reaction temperature and the reaction time will possibly play roles in the final compound of this reaction. The reaction pathways and thus the final properties of the hydrogen treated TiO_2 nanomaterials will be different depending on the hydrogen treatment conditions. The chemical properties of nanomaterials are also affected by their size, shape, morphology, surface facets, and defect contents.[79-81] These variables make this reaction even more complicated. Experimentally, black TiO_2 nanomaterials reported in the literature are normally prepared from different groups under different conditions. It is thus reasonable to see variations of their properties and performance and the accompanying explanations. These variations and complexities, on the other hand, also provide us a large extent of flexibility and more opportunities in tuning the chemical/physical properties and performance of black TiO_2 nanomaterials towards our different needs.

Interaction of hydrogen with TiO_2 crystals and surfaces has been studied for a long time.[82-97] For examples, in 1951, Cronemeyer and Gilleo found hydrogen reduced rutile single-crystals had long wavelength absorption,[82] and in 1958, Cronemeyer found rutile single-crystals reduced with hydrogen at 700 °C had the increased electrical conductivity due to the ionization trapped electrons in oxygen vacancies.[85] Hasiguti, et al. suggested the electrical conductivity were mostly Ti interstitial defects.[94,95] Sekiya, et al. found that the color of TiO_2 changed to pale blue or dark blue when annealed in hydrogen, due to the absorption bands from the oxygen vacancy defect states below the fundamental absorption edge.[97] While TiO_2 surfaces were found not strongly interacting

with molecular hydrogen,[88] additional emission peaks in the valence band region were observed with high doses of H_2 even at room temperature,[87] and atomic hydrogen stick to TiO_2 (110) surfaces at room temperature.[90] Reduction occurred when a TiO_2 surface was annealed in a H_2 atmosphere under high vacuum conditions.[89,92] In the following, we will focus on recent studies on the formation of black TiO_2 nanoparticles.

2.1.1 High-pressure pure hydrogen treatment

Chen et al. reported the preparation of black TiO_2 nanoparticles by treating pure white TiO_2 nanoparticles under 20.0-bar pure H_2 atmosphere at about 200°C for 5 days.[75] The pure TiO_2 nanocrystals were obtained by heating the mixture of titanium tetraisopropoxide, Pluronic F127, hydrochloric acid, deionized water, and ethanol, with the molar ratio of 1:0.005:0.5:15:40 at 40°C for 24 hours, followed by drying at 110°C for 24 hours and calcinating at 500°C for 6 hours.[75] Figure 1 shows the schematic illustration of the concept of making black TiO_2 nanomaterials (Figure 1A), along with the pictures (Figure 1B) and high-resolution transmission electron microscopy (HRTEM) images (Figures 1C and 1D) of white and black TiO_2 nanoparticles.[75] Black TiO_2 nanoparticles featured with a well-crystallized lattice core surrounded by a lattice-disordered shell from the hydrogenation treatment.[75,95-97] The disordered shell was believed to host the possible hydrogen dopant, form the Ti-H and O-H bonds, and contributed to the midgap states and the black color of the hydrogenated TiO_2 nanoparticles.[75,95-97] The black hydrogenated TiO_2 nanoparticles had an onset of optical absorption of about 1.0 eV (~1200 nm) and an optical gap around 1.54 eV (806.8 nm) from the UV-visible absorption spectrum (Figure 1E).[75]

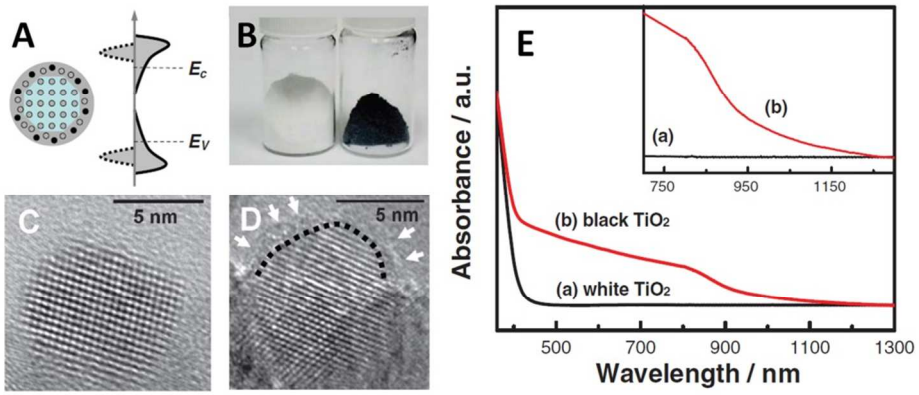

Figure 1. (A) Schematic illustration of the concept to make black TiO_2. (B) Pictures of white and black TiO_2 nanomaterials. High-resolution transmission electron microscopy images of (C) white and (D) black TiO_2 nanoparticles.[75] Reprinted with permission from ref 75. Copyright 2011 AAAS.

Sun et al. (Sun 2011) made black TiO_2 nanoparticles and investigated the hydrogen incorporation into facet-defined anatase TiO_2 nanocrystals under high pressure.[101] They found that hydrogenated TiO_2-(101) and TiO_2-(001) nanocrystals were black (Figures 2A) and blue (Figures 2B), respectively.[101] The amount of hydrogen stored in TiO_2 nanocrystals depended on their facets.[101] Under an initial hydrogen pressure of 7.0 MP at 450 °C, TiO_2 nanocrystals with predominant (101) surface had a storage capacities of 1.4 wt % (Figures 2A), while TiO_2 nanocrystals with (001) surface terminations had a storage capacities of 1.0 wt % (Figures 2B).[101] Hydrogen occupied the interstitial sites between titanium-oxygen octahedra in the lattice and the energy barrier for hydrogen incorporation was lower through the anatase (101) surface than that through (001) (Figures 2C and 2D).[101]

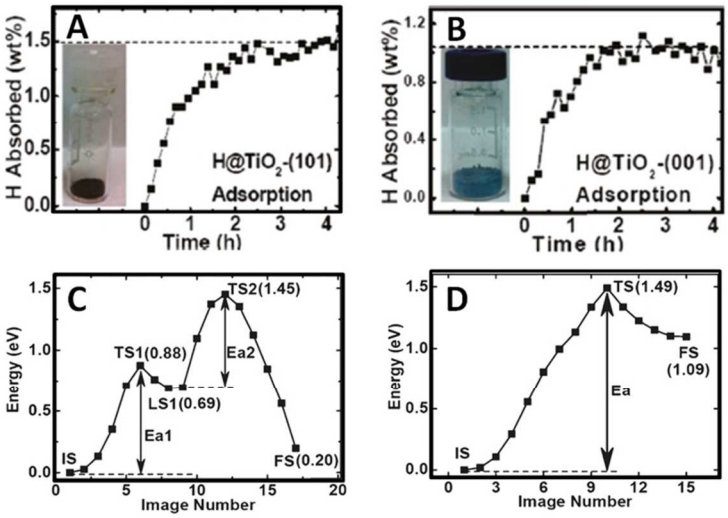

Figure 2. Hydrogen adsorption profiles and digital camera images for (a) TiO_2-(101) and (B) TiO_2-(001). Calculated energy profiles for hydrogen incorporation through (C) (101) and (D) (001) surfaces.[101] Reprinted with permission from ref 101. Copyright 2011, American Chemical Society.

Lu et al. prepared black TiO_2 nanoparticles at room temperature under high-pressure H_2 environment and studied the color change of the hydrogenated TiO_2 nanoparticles over time.[102] The hydrogenation reaction was conducted by hydrogenating commercial P25 TiO_2 powders (0.5 g) under 35 bar hydrogen atmosphere at room temperature (about 15 °C) for 0-20 days.[102] The color of the white P25 turned into pale yellow after hydrogenation for 3 days' hydrogenation.[102] Its color became much darker with a longer hydrogenation time and turn into gray after treatment for 15 days.[102] Black TiO_2 nanoparticles were obtained after hydrogenated for more than 15 days.[102] The black TiO_2 has a crystalline disordered core-shell structure.[102] The corresponding visual and optical absorption property changes are shown in Figure 3.[102] The onset of the optical

absorption of the black TiO_2 nanoparticle was about 1.0 eV and an abrupt bandgap absorbance occurred at about 1.82 eV (680 nm).[102]

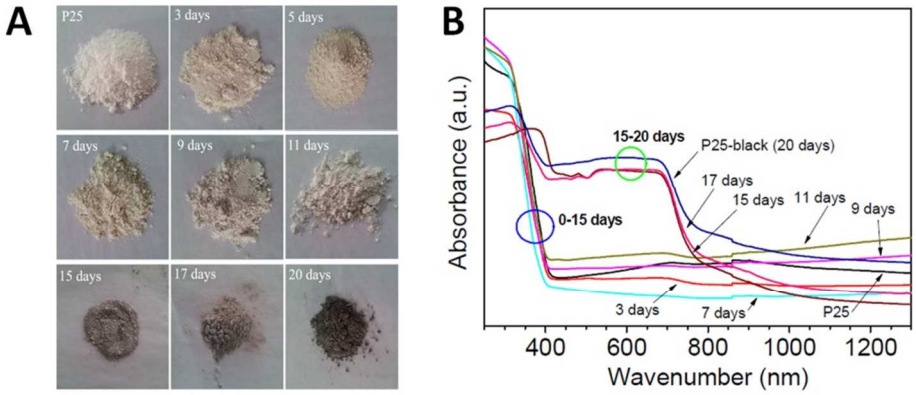

Figure 3. (A) Pictures and (B) UV-visible absorption spectra of hydrogenated TiO_2 nanoparticles over various hydrogenation time.[102] Reprinted with permission from ref 102. Copyright 2014, The Royal Society of Chemistry.

Liu et al compared the color change of anatase TiO_2 nanotubes hydrogenated under various conditions: (i) an anatase TiO_2 nanotube layer (air); (ii) this layer converted with Ar (Ar) or H_2/Ar (H_2/Ar); (iii) a high pressure H_2 treatment (20 bar, 500 °C for 1 h) (HP-H_2); and (iv) a high pressure H_2 treatment but mild heating (H_2, 20 bar, 200 °C for 5 d).[103] After the reduction treatments, the color of the TiO_2 nanotubes turned from white into black in H_2/Ar, deep purple in pure Ar (500 °C for 1 h), light blue in pressurized H_2 at high temperature (20 bar, 500 °C for 1 h), and gray in pressurized H_2 at mild temperature (H_2, 20 bar, 200 °C for 5 d), as shown in Figure 4, which also displays their UV-visible absorption spectra.[103] Apparently, the hydrogenation condition played a critical role in the final color and optical properties of the hydrogenated TiO_2 nanotubes.[103] The original TiO_2 nanotubes were obtained by anodizing a Ti foil with a Pt

counter electrode in ethylene glycol with addition H_2O (1 M) and NH_4F (0.1 M) at 60 V for 15 min, followed by annealing at 450 °C for 1h.[103]

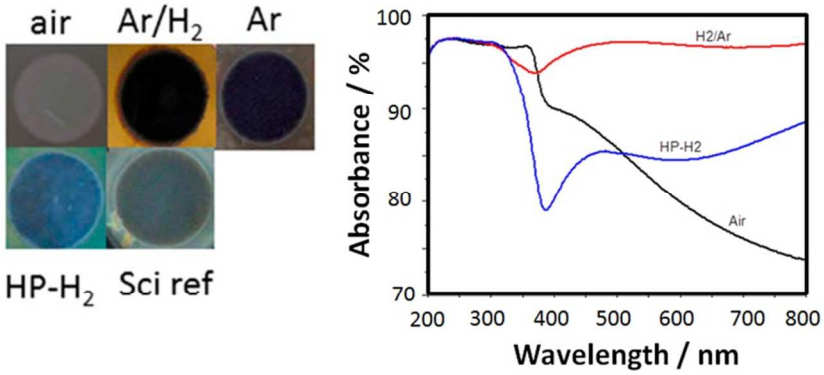

Figure 4. Images and the UV-visible absorption of of the TiO_2 nanomaterials treated under various conditions.[103] Reprinted with permission from ref 103. Copyright 2014, American Chemical Society.

Qiu et al. prepared blue hydrogenated rutile TiO_2 nanoparticles by heating rutile TiO_2 nanoparticles (40 nm) under 40 bar hydrogen pressure at 450 °C for 1 h.[104] The white rutile TiO_2 nanoparticles turned into blue color after 5 min's hydrogenation.[104] Its blue color became more intense with increased reaction time and subsequently steady after 30 min's reaction.[104] The blue color changed into gray after the hydrogenated rutile TiO_2 nanoparticles were exposed to the air.[104] Qiu et al. also fabricated blue hydrogenated lithium titanate by treating lithium titanate at 500 °C for 1 h under a 40 bar H_2 atmosphere.[105] The blue color of the hydrogenated lithium titanate was stable in air.[105]

Wang et al. studied the hydrogenation of F and N-F doped anatase TiO_2 nanoparticles dominated with {001} facets.[106-108] The hydrogenation was performed at 400 °C for 2 h under 10 bar pure H_2 atmosphere to create hydrogenated F and N-F doped

TiO_2 (TiO_2-HF and TiO_2-NHF).[108] The F doped TiO_2 (TiO_2-F) were prepared by reacting $Ti(OBu)_4$ (25 ml) with HF (6 ml) and water (9 ml) at 180 °C for 24 h in an autoclave.[108] N dopant was introduced by reacting with urea at 400 °C for 2 h in air to obtain N-F doped TiO_2 (TiO_2-NF).[108] As shown in Figure 5, The colors of TiO_2-F, TiO_2-NF, TiO_2-HF, and TiO_2-NHF were white, yellow, blue and brown color, respectively.[108] TiO_2-F only showed absorption in the UV region, TiO_2-NF had an onset of absorption around 590 nm, TiO_2-HF showed increased visible-light absorption from 500 nm to 1000 nm, and TiO_2-NHF had a small and flat visible-light absorption from 400 nm to 1000 nm.[108]

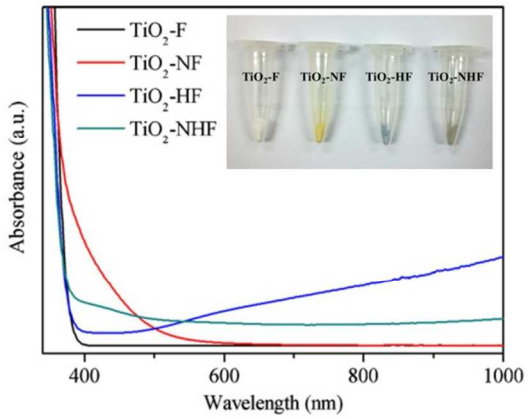

Figure 5. UV–visible absorption spectra and pictures of TiO_2-N, TiO_2-NF, TiO_2-HF, and TiO_2-NHF.[108] Reprinted with permission from ref. 108. Copyright 2012, Elsevier.

Leshuk et al. conducted hydrogenation under a 300 ± 5 psig pure H_2 gas environment at 200 °C for 5 days or under a 10% H_2 + 90% Ar gas flow at 400 – 500 °C for 24-102 h on various TiO_2 nanomaterials.[109,110] They found that under both hydrogen gas environments the color of the hydrogenated TiO_2 nanomaterials changed to yellow or black, depending on how the original TiO_2 nanomaterials were prepared.[110]

2.1.2 Ambient or low-pressure pure hydrogen treatment

Rekoske, et al. reported that reduction of anatase and rutile TiO_2 with H_2 at 300 – 500 °C under ambient hydrogen pressure, however, they did not mention the optical properties.[111] In 2003, Liu et al. treated anatase TiO_2 nanoparticles (30 nm in diameter) under pure H_2 flow with general grade from 20 to 700 °C for 2 h, however, no report was available on the optical and color property changes.[112] Yu et al performed hydrogenation on anatase TiO_2 nanosheets under a H_2 gas flow (50 sccm) at atmospheric pressure in a quartz tube at 500 – 700 °C for various time.[113] The TiO_2 nanosheets were prepared by treating tetrabutyl titanate (25 g) with HF (4 mL) at 200 °C for 24 h.[113] The color of the nanosheets changed from white to blue, then finally to gray, depending on the hydrogenation temperature and time, as shown in Figure 6A.[113] Figure 6B shows their corresponding UV-visible absorption spectra.[113]

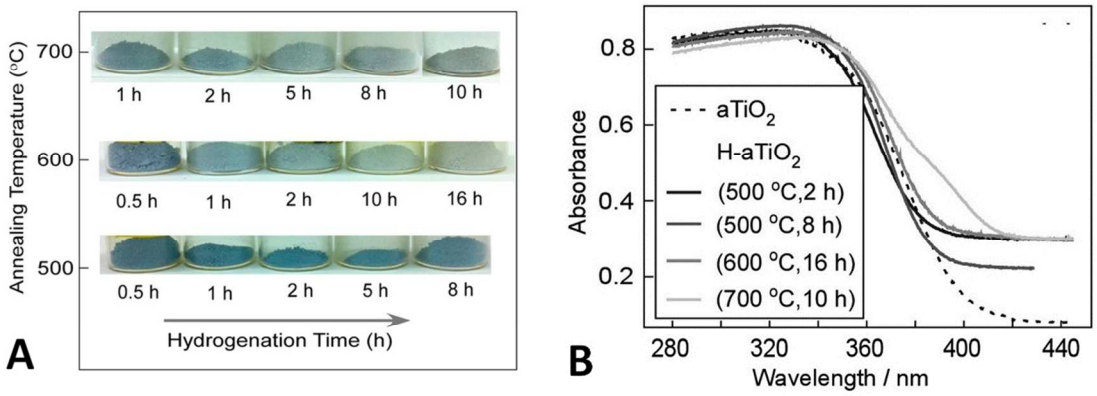

Figure 6. (A) Photographs and (B) UV-visible absorption spectra of hydrogenated anatase TiO_2 nanosheets (H-aTiO_2) prepared with a H_2 gas flow at temperatures of 500 – 700 °C.[113] Reprinted with permission from ref 113. Copyright 2014, American Chemical Society.

Li et al. prepared hydrogenated mesoporous anatase TiO_2 microspheres via a hydrogenation treatment process.[114] The hydrogen thermal treatment was performed by calcining the TiO_2 microspheres under ambient hydrogen pressure at 400 °C for 1 h.[114] The color of the TiO_2 microspheres changed to gray from white after hydrogenation and the hydrogenated TiO_2 microspheres exhibited a high and broad light absorption band towards the infrared region in contrast to the UV absorption of the original TiO_2 microspheres from the UV-visible diffuse reflectance spectra.[114] Lu et al. performed the hydrogenation on anodized TiO_2 nanotubes in ultrahigh purity hydrogen atmosphere (ambient pressure) between 300 to 600 °C for 1 h.[115] However, no information on the color or optical properties was available for the hydrogenated TiO_2 nanotubes.[115] The TiO_2 nanotubes were obtained by anodizing Ti fiber at 30 V for 3 h at room temperature with a graphite rod as cathode in a glycerol aqueous solution (90 vol% glycerol: 10 vol% H_2O) containing 0.75% NH_4F, followed by drying at 80 °C.[115] Similarly, Li et al prepared hydrogenated TiO_2 nanotubes (mainly rutile, 95%) via the anodization of a titanium sheet followed by a hydrogenation process conducted at 450 °C for 2 h in a hydrogen atmosphere (ambient pressure).[116] The TiO_2 nanotubes were obtained by anodizing a Ti foil in 1,2,3-propanetriol containing NH_4F (1.0 wt %) and H_2O (15 vol %) at 25 V for 2 h with a platinum mesh as a cathode, followed by heating at 700 °C for 1 h.[116] Zhang et al. fabricated hydrogenated anatase TiO_2 nanotubes by annealing the anatase TiO_2 nanotubes in ultrahigh purity H_2 atmosphere at 200 – 600 °C for 1 h.[117] The anatase TiO_2 nanotubes were synthesized anodizing a Ti sheet at 50 V for 3 h at room temperature in glycol aqueous solution (90 wt% glycerol: 10 wt% H_2O) containing NH_4F (0.5 wt%).[117]

Wang et al. prepared hydrogenated rutile TiO_2 nanowire arrays by annealing in ultrahigh purity hydrogen atmosphere (ambient pressure) for 3 h at 200 – 550 °C.[118] The color of the hydrogenated rutile TiO_2 nanowires turned into yellowish green (350 °C) and black (450 °C or above), depending on the hydrogen annealing temperature (Figure 7).[118] This suggested that the hydrogenated rutile TiO_2 nanowires had visible light absorption as a result of hydrogen treatment.[118] The original rutile TiO_2 nanowires were obtained by treating titanium n-butoxide (0.5 ml) in HCl (18.25%) solution at 150 °C for 5 hours, followed by annealing in air at 550 °C for 3 h.[118]

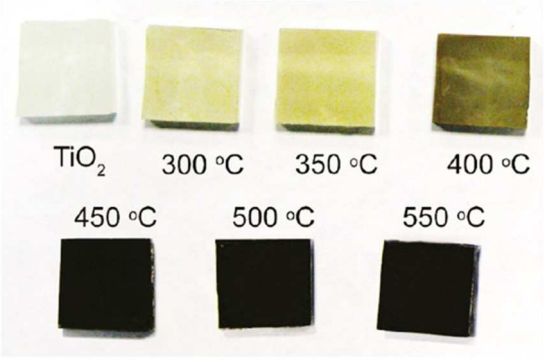

Figure 7. Pictures of rutile TiO_2 nanowires hydrogenated at various temperatures for 3 h.[118] Reprinted with permission from ref 118. Copyright 2011, American Chemical Society.

Naldoni et al. prepared black TiO_2 nanoparticles by heating amorphous TiO_2 under H_2 stream, followed by fast cooling in inert environment until room temperature.[119] They treated amorphous TiO_2 powders under vacuum (10^{-5} mbar) and then heated at 200 °C for 1 h under flowing O_2, and then heated 500 °C for 1 h under hydrogen atmosphere.[119] They found that the use of very slow cooling rate or instantaneous

exposure to air resulted in a gray coloration, and that reducing crystalline samples generated only pale blue colored powders with unmodified absorption spectra.[119]

Barzan et al. conducted the hydrogenation reaction on P25 under pure hydrogen atmosphere (pressure of 200 mbar) at 500 °C for 1 h and obtained TiO_2 with blue color.[120] Jiang et al. performed hydrogenation on commercial P25 powders in a tube furnace filled with ultrahigh purity hydrogen gas (99.99%) under atmospheric pressure at 400 °C for 10 h and found that the color of P25 turned into gray.[121] Liang et al. reported the hydrogenation of an anatase TiO_2 inverse opal structure.[122] The hydrogenation reaction was conducted at 500 °C for 2 h under a reduced hydrogen pressure of 80 Torr.[122] However, no information of the optical properties of the hydrogenated TiO_2 was readily available.[122]

2.1.3 Ambient hydrogen/Argon treatment

Shin et al prepared hydrogenated TiO_2 nanoparticles from commercial anatase TiO_2 nanoparticles (50 nm in diameter).[123] The hydrogenation reaction was conducted at 450 °C for 1−7 h under a 5% H_2/ 95% Ar gas flow.[123] They found that the color of pristine TiO_2 changed from pure white (Figure 8A) to light yellowish after 1 h of hydrogen thermal treatment and after 7 h of hydrogen thermal treatment, the color turned to dark yellow (Figure 8B).[123] No color change was visible after the same time of thermal annealing under inert atmosphere.[123]

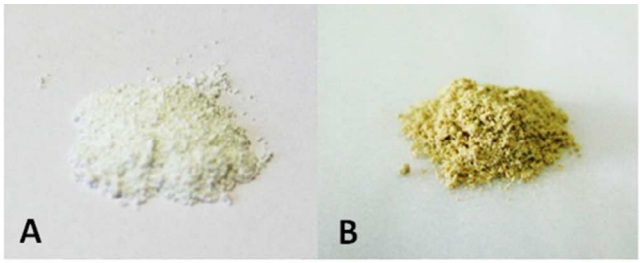

Figure 8. Pictures of anatase TiO_2 before (A) and after (B) hydrogenation for 7 h at 450 °C under a 5% H_2/ 95% Ar gas flow.[123] Reprinted with permission from ref 123. Copyright 2012, American Chemical Society.

Zhu et al. conducted hydrogenation on anatase TiO_2 nanotubes in a quartz tube under a continuous hydrogen (8 sccm) and argon (10 sccm) flux for 5 h at 400 – 600 °C.[124] The anatase TiO_2 nanotubes were obtained from anodization of Ti foil in an ethylene glycol solution containing NH_4F (0.25 wt%) and HF (0.02 wt%) at 40 V at room temperature for 40 min.[124] However, no information on the optical properties was provided in this study.[124] Lu et al reported hydrogenation on anatase nanoparticles, anatase nanotubes and rutile nanorods.[125] The hydrogenation was carried out by annealing various TiO_2 nanomaterials at 450 °C for 1 h in a reducing 5% H_2 and 95% Ar atmosphere (100 sccm flow rate).[125] The hydrogenated TiO_2 nanomaterials turned into black from white (Figure 8).[125] The original TiO_2 nanotubes were prepared by anodizing Ti foil in ethylene glycol with 0.5 wt% ammonium fluoride and 4–6 vol% water at a constant potential of 60 V for 0.5 h, followed by annealing at 500 °C for 3 h.[125] The starting rutile TiO_2 nanorods were made by heating titanium n-butoxide (0.5 ml) in HCl (18.25%) solution at 150 °C for 5 hours, followed by annealing in air at 550 °C for 3 h.[125] The anatase TiO_2 nanoparticles were bought from Aldrich with grain size of 50 nm.[125]

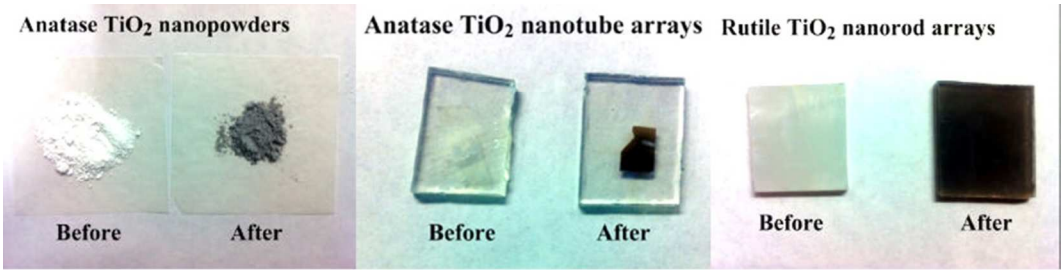

Figure 9. Pictures of anatase TiO_2 nanoparticles, nanotubes, and rutile nanorods before (A) and after (B) hydrogenation at 450 °C for 1 h under a 5% H_2/ 95% Ar gas flow.[125] Reprinted with permission from ref 125. Copyright 2012, Wiley-VCH.

Shen et al. performed hydrogenation on lithium titanate nanowires.[126] The hydrogenation was conducted by treating the nanowires at 500 – 700 °C for 1.5 h in 5% v/v H_2/Ar.[126] The titanate nanowires were prepared by reacting a titanium foil (1 cm × 2 cm) in 1 M NaOH (20 mL) aqueous solution at 220 ° C for 16 h in an autoclave, followed by immersion in 0.5 M HCl solution for 1 h and 2 M LiOH solution for 8 h at 60 °C.[126] Danon et al. treated titanate nanotubes under a flow of 5% H_2 in Ar at atmospheric pressure at 350 °C for 3 h and found that in stainless reactor, black powders were obtained, but in quartz reactor, only blue powders were synthesized, as shown in Figure 10.[127] The starting titanate nanotubes were prepared by heating anatase TiO_2 powders (2 g) in a of 10M NaOH solution (50 mL) 120 °C for 48 h, following by washing with 1M HCl, water and drying at 110 °C overnight.[127]

Figure 10. Pictures of titanate nanotubes and after hydrogenation at 350 °C for 3 h under a flow of 5% H_2 in Ar at atmospheric pressure in a stainless reactor and a quartz reactor.[127] Reprinted with permission from ref 127. Copyright 2012, American Chemical Society.

Zhang et al prepared hydrogenated rutile TiO_2 nanorods by treating rutile TiO_2 nanorods in a H_2/Ar flow.[128] The hydrogenation process was carried out in a hydrogen (20 sccm) and argon (80 sccm) atmosphere at 350 °C in a tubular furnace under ambient pressure for 1 h.[128] The starting TiO_2 nanorods were prepared on a fluorine-doped tin oxide glass slide by reacting titanium butoxide (0.48 mL) in HCl solution (40 mL 18.25 wt%) at 170 °C for 6 h.[128] The hydrogenated TiO_2 nanorods had a stronger absorbance in the visible light region (ca. 50%) than and a slight enhancement in the UV light region (ca. 4%), compared to pristine TiO_2 nanorods.[128]

Zeng et al carried out hydrogenation on pure and C-doped TiO_2 nanoparticles under a flow of H_2/Ar mixture at 300 °C for 2h,[129] however, did not report on their optical properties. Wang et al. synthesized hydrogenated TiO_2–reduced-graphene oxide nanocomposite.[130] Typically, tetrabutyl titanate was added into ethanol containing graphene oxide and reacted at 90 °C for 8 h.[130] The powder was treated at 450 °C for 4 h under a 5% H_2/95% Ar flow.[130]

Hoang et al prepared N, H-doped rutile TiO_2 nanowires via hydrothermal synthesis followed hydrogenation treatment.[131] The rutile TiO_2 nanowires were prepared in 50 mL n-hexane, 5 mL HCl, and 5 mL of titanium (IV) isopropoxide at 150 °C for 5 h on seeded fluorine-doped tin oxide substrates.[131] The nanowires were annealed at 500 °C (i) in air for 1 h (denoted as TiO_2), (ii) in NH_3 for 2 h (N-TiO_2), (iii) in a mixture of H_2 and Ar (5% of H_2) for 1 h (H-TiO_2), and (iv) in a mixture of H_2 and Ar for 1 h followed by annealing in NH_3 for 2 h (H, N-TiO_2).[131] As shown in Figure 11, the color of the pristine TiO_2 nanowires did not change after hydrogen treatment; however, it turned green after nitridation and dark green after hydrogenation-nitridation treatment.[131] The hydrogenated TiO_2 nanowires had increased absorption in both UV and visible light region compared to the pristine TiO_2 nanowires, and the absorption edge of the H, N-TiO_2 nanowires shifted ~20 nm to the longer wavelength region compared to the N-doped TiO_2 nanowires.[131]

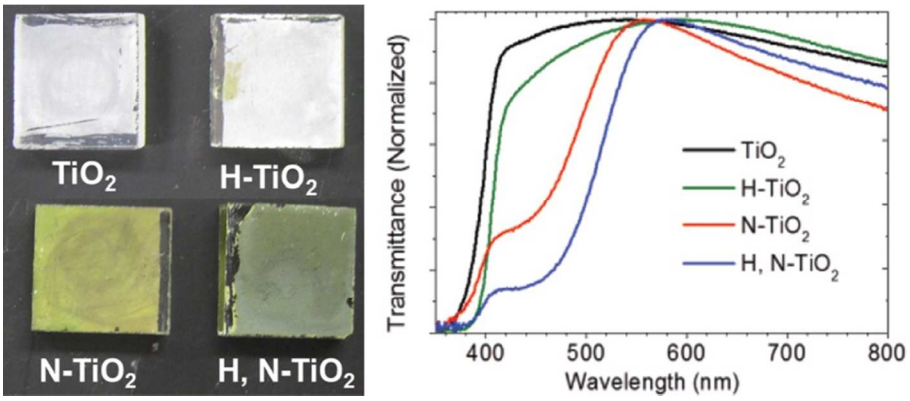

Figure 11. Pictures and UV-visible transmission spectra of various TiO_2 nanowires.[131] Reprinted with permission from ref 131. Copyright 2012, American Chemical Society.

2.1.4 Ambient hydrogen/nitrogen treatment

He et al prepared hydrogenated TiO_2 nanostructured film by annealing the TiO_2 film at 350 °C for 2 h in a mixed gas of 6% H_2 and 94% N_2.[132] The hydrogenated TiO_2 nanostructured film had a yellow color while the TiO_2 film was transparent (Figure 12).[132] The H:TiO_2 film showed a stronger absorption than pure TiO_2 film in both UV and visible light regions (Figure 12).[132] The pristine TiO_2 nanoparticles were obtained by heating titanium isopropoxide (0.02 M), acetic acid (0.02 M), H_2O (27.4 ml) and HNO_3 (0.4 ml 80%) at 200 °C for 12 h after stirring at 80 °C for 2 h.[132] The nanostructured TiO_2 films were fabricated by screen printing of a TiO_2-terpineol-ethylcellulose ethanol slurry on fluorine-doped tin oxide glasses, followed by annealing at 500 °C for 30 min.[132]

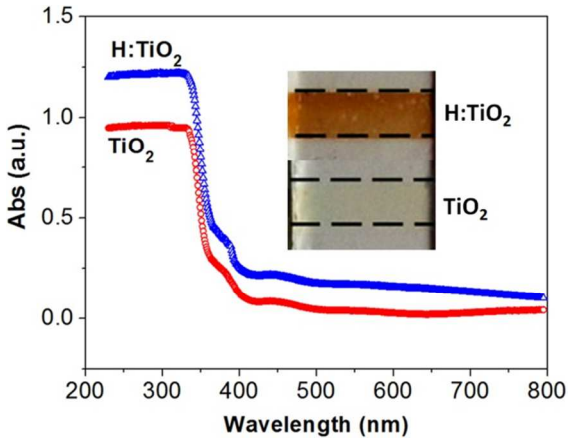

Figure 12. UV-visible absorption spectra of pristine (TiO_2) and hydrogenated (H:TiO_2) TiO_2 nanostructured films.[132] The inset shows their pictures and the Reprinted with permission from ref 132. Copyright 2013, American Institute of Physics.

Wang et al. conducted hydrogen treatment on rutile TiO_2 nanorods with anatase nanoparticles.[133] The hydrogenation reaction was conducted at 400 °C for 30 minutes in a mixed gas of 90% N_2 and 10% H_2.[133] The color of the film changed from white to gray after annealing.[133] The TiO_2 nanorods were prepared by heating 1.5 ml mixed solution of

hydrochloric acid (47.2 vol.%), deionized water (51.5 vol.%), and tetrabutyl titanate (1.3 vol.%) in an autoclave at 150 °C for 10 h, followed by heating at 450 °C for 30 minutes.[133] The anatase nanoparticles were then loaded in a 0.04 M $TiCl_4$ aqueous solution at 70 °C for 12 h in an autoclave.[133] Zheng et al hydrogenated anatase TiO_2 nanowire microspheres at 500 °C for 4 h under a flow of H_2 (5 % in N_2, 300 sccm).[134] The color of the hydrogenated anatase TiO_2 nanowire microspheres was dark brown compared to the white color of the pristine microspheres, and had enhanced visible-light absorption.[134] The nanowire-microspheres were obtained by heating $Ti(OBu)_4$ (5.1 g) in ethanol (75 mL) with sulfuric acid (0.33 mL, 98%) and water (0.3 mL) at 180 °C for 4 h in an autoclave, followed by heating at 150 °C for 24 h in 10 M NaOH aqueous solutions and ion-exchanged in 0.1 M HCl aqueous solution for 12 h.[134]

Zhu et al prepared black TiO_2 through hydrogen spill on supported Pt nanoparticles (Figure 13).[135] Hydrogenated Pt/TiO_2 was obtained by treating Pt/P25 in a 8% H_2/N_2 atmosphere at 200 – 700 °C for 4 h.[135] Pt/P25 was first prepared via conventional impregnation followed by reduction with sodium borohydride.[135] The hydrogenation reduction started from 160 °C, and became apparent at 400, 500, 700 and 750 °C due to the hydrogen spillover from Pt to TiO_2.[135] The hydrogenated TiO_2 nanoparticles had large visible-light absorption then the pristine TiO_2 nanoparticles.[135]

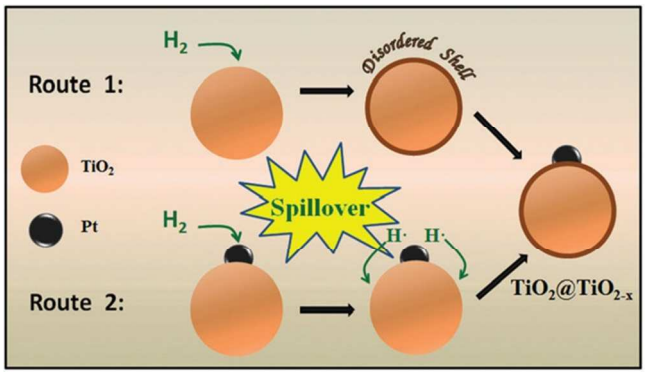

Figure 13. Illustration of routes to prepared hydrogenated Pt/TiO_2 nanoparticles. Route 1: hydrogenation of TiO_2 followed by the loading of Pt; route 2: hydrogen spillover involved simultaneous hydrogenation of Pt/TiO_2.[135] Reprinted with permission from ref 135. Copyright 2014, The Royal Society of Chemistry.

2.1.5. Ambient Argon treatment

Myung et al. prepared black TiO_2 nanoparticles by annealing a yellow TiO_2 gel in Ar gas at 400 – 600 °C for 5 h.[136] The TiO_2 gel was obtained by stirring high-purity $TiCl_4$ dropwise to a distilled water-ethanol mixture with HF and urea at 0 °C for 4 h, and then evaporating the solution slowly at 80 °C.[136] The color of the annealed TiO_2 nanoparticles depended on the annealing temperature and the amount of HF added in the preparation of the TiO_2 gel.[136]

2.2 Hydrogen plasma

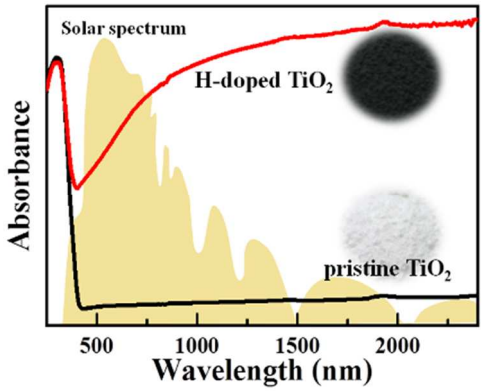

Figure 14. UV-visible-IR absorption spectra and pictures of the pristine and hydrogen plasma treated black TiO_2 nanoparticles.[137] Reprinted with permission from ref 137. Copyright 2013, Wiley-VCH.

Wang et al. prepared hydrogenated black TiO_2 nanoparticles in a thermal plasma furnace by hydrogen plasma for 4 - 8 h at 500 °C.[137] The plasma input power was 200 W and the starting TiO_2 was P25.[137] The hydrogenated black TiO_2 nanoparticles had a significant absorption in the visible and near infrared light (Figure 14).[137] Their absorption in the visible and infrared light region increased drastically and monotonously with wavelengths longer than ≈ 400 nm.[137] Teng et al. prepared of black TiO_2 nanotubes by hydrogen plasma assisted chemical vapor deposition.[138] The hydrogenation was performed in a hot-filament chemical vapor deposition apparatus with hydrogen as reaction gas (Figure 15A).[138] The TiO_2 nanotubes were obtained by heating 2 g of Degussa P25 nanoparticles (2 g) in 10 M NaOH solution (50 mL) at 120 °C for 12 h, followed by washing with HCl and water, and drying at 110 °C.[138] During the treatment process, the TiO_2 was loaded in a corundum boat under the filament.[138] The temperature of the filament was maintained at 2000 °C, and the samples were treated for 3 h at 350 -

500 °C (TiO_2-350, TiO_2-500).[138] Some Cr fragments were mixed in the TiO_2 during the treatment process to study the effect of Cr (TiO_2-Cr-350, TiO_2-Cr-500).[138] All the hydrogenated TiO_2 nanoparticles had black color (Figure 15B) and enhanced absorption in the visible-light region (Figure 15C).[138] Yan et al also prepared hydrogenated black anatase TiO_2 nanoparticles by a H_2 plasma treatment.[139] The H_2 plasma treatment was performed at 390 °C for 3 h, with the inductively coupled plasma power of 3000 W, the chamber pressure of 26.5–28.3 mTorr, and the H_2 flow rate of 50 sccm. The starting anatase TiO_2 nanoparticles had a mean diameter of 15 nm.[139] The hydrogenated TiO_2 nanoparticles had black color and increased absorption in the visible-light region (Figure 15D).[139]

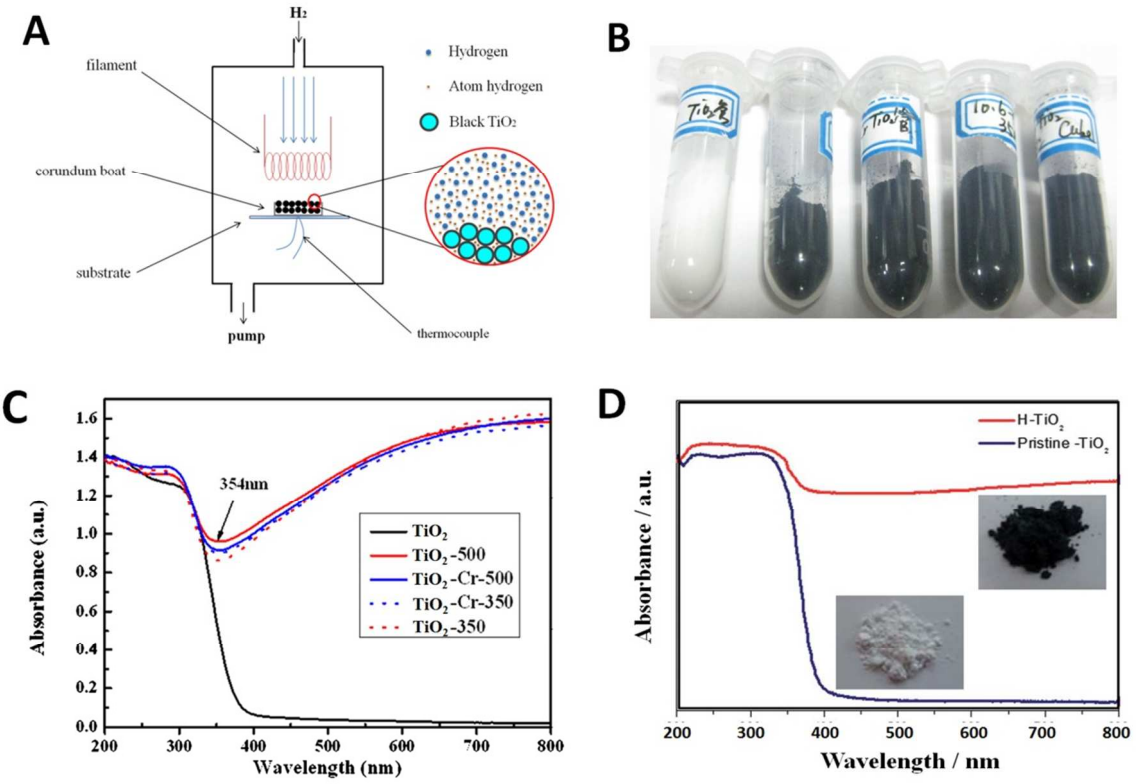

Figure 15. (A) Illustration of hydrogen plasma hot-filament chemical vapor deposition setup. (B) Pictures and (C) UV-visible absorption spectra of the pristine and

hydrogenated black TiO_2 nanoparticles.[138] Reprinted with permission from ref 138. Copyright 2014, Elsevier. (D) Pictures and UV-visible absorption spectra of the pristine and hydrogenated black TiO_2 nanoparticles.[139] Reprinted with permission from ref 139. Copyright 2013, The Royal Society of Chemistry.

2.3 Chemical reduction

2.3.1 Aluminum reduction

Wang et al. prepared black TiO_2 nanoparticles using Al as a reductant in an evacuated two-zone vacuum furnace at 300 – 500 °C.[140] For the reduction reaction, TiO_2 and aluminum were placed separately in a two-zone tube furnace and then evacuated to a base pressure lower than 0.5 Pa (Figure 16A).[140] The aluminum was heated at 800 °C, and TiO_2 samples were heated at 300 - 600 °C for 6 - 20 h.[140] The aluminum sustained low oxygen partial pressure from melting and releasing the O from TiO_2.[140] The reduced TiO_2 nanoparticles had black color (Figure 16B), and showed intense absorption in the visible-light and near-infrared regions.[140]

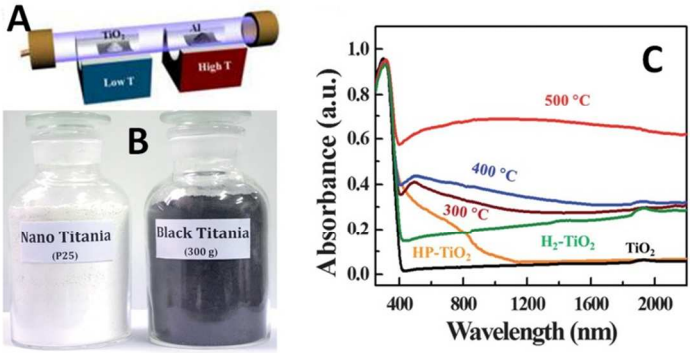

Figure 16. (A) Schematic illustration of the two-zone furnace, (B) Pictures and (B) UV-visible absorption spectra of TiO_2 nanoparticles reduced at different temperatures (300 °C, 400 °C, and 500 °C) by Al, the high-pressure hydrogenated black TiO_2 (HP-TiO_2), the

H_2-reduced TiO_2 (H_2–TiO_2), and pristine TiO_2.[140] Reprinted with permission from ref 140. Copyright 2013, The Royal Society of Chemistry.

Cui et al. prepared black anatase TiO_2 nanotubes by the melted aluminum reduction of pristine anodized and air-annealed TiO_2 nanotube arrays.[141] In the reduction process, TiO_2 nanotubes and aluminum powder were heated to 500 °C and 850 °C for 4 h, respectively.[141] The TiO_2 nanotubes were prepared by anodizing an Ti foil with copper plate as the cathode in a glycol electrolyte containing 0.4 wt% NH_4F and 3 wt% H_2O under 100 V for 5 min, after peeling off the first layer obtained under 100 V for 25 min and followed by annealing at 500 °C for 4 h in air.[141] The black anatase TiO_2 nanotubes had large absorption from visible-light to near-infrared regions.[141]

Yin et al prepared gray anatase TiO_2 nanowires by treating protonated titanate nanowires (0.5 g) under vacuum at 200 – 900 °C for 4 h in a two-zone furnace under Al atmosphere where aluminum powder was put in the zone set at 800 °C.[142] The protonated titanate nanowires were prepared with hydrothermal reaction of anatase powder in 10 M NaOH solution at 200 °C for 18 h.[142] The gray nanowires exhibited stable visible-light and even infrared light absorption.[142]

Similarly, Zhu et al. to synthesized black brookite TiO_2 nanoparticles in a two-zone vacuum furnace with the Al reduction method.[143] The Al powders and brookite TiO_2 were separately heated at 800 °C (Al) and 300 – 600 ºC (brookite) for 4 h in a two-zone evacuated furnace under a pressure of 0.5 Pa.[143] The brookite TiO_2 nanoparticles were synthesized heating at 220 ºC for 48 h under pH 12.5 the precipitates from the reaction of

$TiOSO_4 \bullet xH_2O$ (3 g) and 10 M NaOH (6.25 ml) in water (50 ml).[143] The black brookite TiO_2 had drastically enhanced visible and infrared light absorption.[143]

Yang et al. synthesized black core-shell rutile TiO_2 nanoparticles with sulfided surface (TiO_{2-x}:S) from both anatase and rutile nanoparticles.[144] Rutile (route 1) and anatase (route 2) TiO_2 with sizes of ~30 nm in diameter were first reduced by molten Al to form a disordered TiO_{2-x} shell (Figure 17A).[144] The Al powders and pristine TiO_2 were separately heated at 800 °C (molten Al) and 500 °C (TiO_2) for 6 h in an evacuated two-zone furnace under 5×10^{-4} Pa pressure.[144] The modified TiO_2 nanoparticles were treated at 600 °C for 4 h in a 1000 Pa H_2S.[144] This sulfided rutile TiO_2 nanoparticles exhibited remarkably enhanced absorption in visible and near-infrared regions (Figures 17B and 17C).[144] The color of the sulfided rutile TiO_2 nanoparticles was brown or black, depending on the crystal phase of the starting TiO_2 nanoparticles (Figure 17C).[144] The black color changed into gray after annealing.[144]

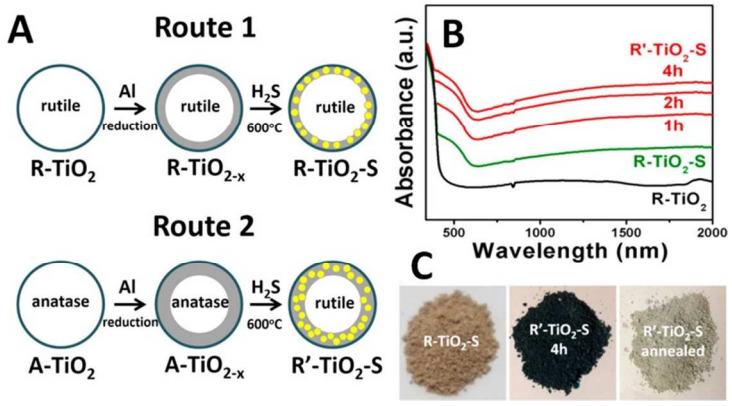

Figure 17. (A) Illustration of routes 1 and 2 to make black core-shell rutile TiO_2 nanoparticles with sulfided surface. (B) UV-visible absorption spectra of TiO_2 and sulfided rutile and anatase TiO_2 nanoparticles. The sulfided rutile and anatase

nanoparticles were labeled as R-TiO_2-S and R′-TiO_2-S, respectively.[144] Reprinted with permission from ref 144. Copyright 2013, American Chemical Society.

Lin et al. further synthesized a series of nonmetal-doped black titania with this two-step strategy (Figure 18).[145] First, reduction by molten Al introduced oxygen vacancies on the amorphous surface layer surrounding the crystalline core in TiO_2 (Degussa P25) nanocrystals.[145] Then incorporation nonmetal element X (X = H, N, S, I) in the oxygen-deficient amorphous layers of Al-reduced titania nanocrystals (TiO_{2-x}) induced color change.[145] The P25 (0.5 g) and aluminum powders were treated at 500 °C and 800 °C for 6 h, respectively, in a two-zone evacuated furnace, under the pressure of 0.5 Pa, to obtain black TiO_{2-x} nanoparticles.[145] The hydrogenation was then performed in a thermal plasma furnace by hydrogen plasma at 500 °C for 4 h.[145] The TiO_2–S and TiO_2–I were prepared by reacting black TiO_{2-x} nanoparticles with S and I_2 at 500 °C for 4 h, respectively, followed by dispersed in CS_2 (ethanol for I_2) solution to remove residual S (I_2) to obtain TiO_2–S (TiO_2–I) nanoparticles.[145] The black TiO_2-N nanoparticles were obtained by heating black TiO_{2-x} nanoparticles in a NH_3-Ar (2:1) gas flow at atmospheric pressure at 500 °C for 4 h.[145] All the TiO_2-X nanoparticles displayed enhanced absorption in both visible-light and near-infrared regions.[145] The amount of light absorbed followed in this order: TiO_2-N > TiO_2-S > TiO_2-I > TiO_{2-x} > TiO_2-H > TiO_2.[145]

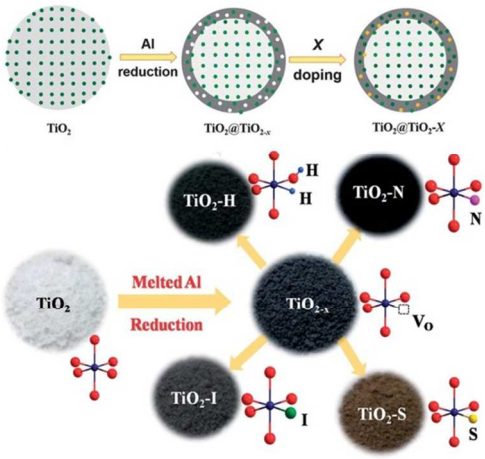

Figure 18. Schematic evolution from pristine TiO_2 to oxygen-deficient titania (TiO_{2-x}) and then to X-doped titania (TiO_2-X: X = H, N, S, I).[145] Reprinted with permission from ref 145. Copyright 2013, The Royal Society of Chemistry.

2.3.2 Zinc reduction

Zhao et al prepared reduced gray rutile TiO_2 nanoparticles with zinc reduction in a solvothermal route.[146] Typically, $TiCl_3$ (1 mL, 15 – 20%) aqueous solution was reacted in isopropanol (30 mL) in the presence of Zn powders (0.5 – 2.5 mmol) at 180 °C for 6 hours.[146] The excess Zn powders were removed with HCl aqueous solution.[146] Zn powders were added to avoid the complete oxidation of Ti^{3+} in the reaction.[146] Without Zn powers, only white anatase TiO_2 was obtained.[146] The color of TiO_2 can be changed from gray to dark blue depending on the amount of Zn (the inset in Figure 18).[146] The reduced TiO_2 nanorods showed a broad visible-light absorption band, which increased with the addition of Zn powder in the reaction (Figure 19).[146] Meanwhile, the relative amount of rutile phase increased with the amount of Zn powder.[146]

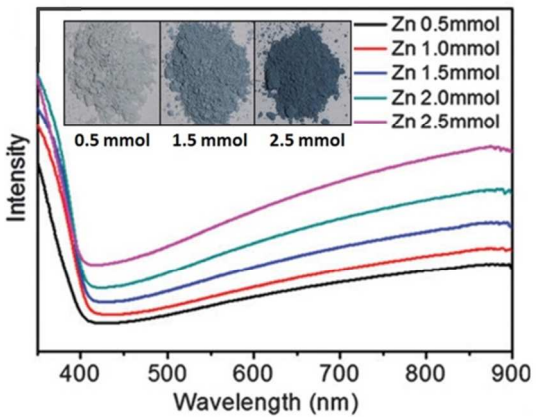

Figure 19. UV-visible absorbance spectra and pictures of TiO_2 nanoparticles by Zn reduction.[146] Reprinted with permission from ref 146. Copyright 2014, The Royal Society of Chemistry.

2.3.3 Imidazole reduction

Zou et al prepared reduced gray TiO_2 nanoparticles by calcining a mixture of a porous amorphous TiO_2 precursor (0.5 g), imidazole (1 g), and hydrochloric acid (37 wt%, 3 mL) in a preheated muffle furnace (450 °C) for 6 h.[147] The amorphous TiO_2 precursor was obtained by photodecomposing titanium glycolate (2.0 g) dispersed in water (60 mL) under UV-light irradiation (for 1 h).[147] The reduced TiO_2 had a broad and strong absorption through the entire visible-light region.[147]

2.3.4 $NaBH_4$ reduction

Kang et al synthesized reduced black TiO_2 nanotubes by chemical reduction with $NaBH_4$.[148] The starting TiO_2 nanotubes were obtained by anodizing a Ti foil in an ethylene glycol solution containing 0.3 wt% NH_4F and 2 vol% H_2O under 80 V for 30 min at 5 °C with a graphite cathode, followed by annealing at 450 °C for 3 h.[148] The

reduction was performed in 0.1 M $NaBH_4$ solution for 10 – 60 min at room temperature.[148] The reduced TiO_2 nanotubes had strong absorption from visible-light region to the near-infrared.[148]

2.3.5 CaH_2 reduction

Tominaka et al. found that black corundum Ti_2O_3 nanoparticles were obtained by reducing of rutile TiO_2 nanoparticles with CaH_2 powder at 350 °C for 10 – 15 d with the same morphology.[149,150]

2.4 Chemical oxidation

Liu et al prepared reduced TiO_{2-x} nanoparticles with a hydrothermal method by oxidizing TiH_2 powder (0.60 g) in H_2O_2 solution (60 mL 25 wt%) at 160 °C for 20-27 h after stirring for 5h at room temperature.[151] The TiO_2 nanoparticles had blue or light-blue color.[151] The particles showed a strong absorption across the UV to the visible light region and retained their light-blue color upon storage in ambient atmosphere or water for one month at 40 °C.[151] Grabstanowicz et al. TiO_2 black powders with a two-step strategy as shown in Figure 20.[152] First, H_2O_2 (15 mL) was added into TiH_2 powder (0.96 g) aqueous suspension (10 mL) and stirred for 3 h at room temperature to obtain a miscible gel-like slurry, followed with additional H_2O_2 (12 mL and 15 mL) and stirring (4 h and 16 h) in forming a yellow gel.[152] Second, the gel was vacuum-desiccated overnight, placed in an oven at 100 °C for 12–20 h to become a yellow powder, and then finally at 630 °C for 3 h in Ar.[152] The black TiO_2 had rutile phase and remarkably enhanced absorption in the visible-light and near-infrared regions.[152] Pei et al. prepared gray TiO_2

by oxidizing TiO powder with a hydrothermal method.[153] In a typical procedure, titanium monoxide (400 mg) was reacted with HCl solution (20 mL 3M) at 160 °C for 24 h.[153] The formed gray TiO_2 showed enhanced and stable absorption across the entire visible-light region.[153] Kako et al. prepared colorful rutile TiO_2 by heating Ti_2O_3 at 550 – 900 °C for 3 h.[154] The samples had colors ranged from grayish green to yellowish off-white and large visible-light absorption.[154]

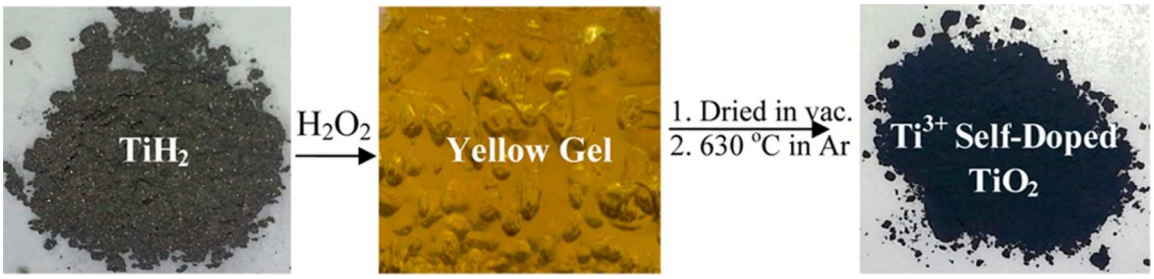

Figure 20. Illustration of the synthesis strategy from TiO_2 to black TiO_2 nanoparticles, along with their images.[152] Reprinted with permission from ref 152. Copyright 2013, American Chemical Society.

2.5 Electrochemical reduction

Xu et al prepared hydrogenated black TiO_2 nanotubes by electrochemically reduction.[155] The nanotubes were obtained by two-step anodization at 150 V for 1 h in ethylene glycol electrolyte containing 0.3 wt.% NH_4F and 10 vol.% H_2O with a carbon rod as the cathode and Ti as the anode.[155] The nanotubes formed after the first-step were removed with adhesive tape to the second anodization.[155] The nanotubes after the second-step were treated at 150 °C for 3 h and at 450 °C for 5 h.[155] The electrochemical reductive doping process was performed under 5 V for 5 to 40 s in 0.5 M Na_2SO_4 aqueous solution at room temperature with the nanotubes as the cathode and a Pt electrode as the anode,

respectively.[155] Zhang et al fabricated black TiO_2 nanotubes with a similar strategy.[156] The TiO_2 nanotubes were obtained by anodizing a Ti sheet at 60 V for 30 min in EG solution containing 0.5 wt% NH_4F and 2 vol% H_2O with a Pt counter electrode, followed by sonicating, another anodizing at 80 V for 5 min, and calcination at 450 °C for 1 h.[156] The reduction was conducted under negative potential (0.4 V vs. reversible hydrogen electrode) in 1 M Na_2SO_4 for 30 min.[156]

Similarly, Li et al prepared black TiO_2 nanotubes using anodization followed by electrochemical reduction as illustrated in Figure 21.[157] TiO_2 nanotubes were first prepared with a Pt gauze as the counter electrode and a Ti foil as the working anode under a constant voltage or current (typically, 80 V for 7200 s, or 4 mA for 5000 s) in an "aged" ethylene glycol solution under 60 V for 12 h with 0.2 M HF and 0.12 M H_2O_2.[157] The nanotubes were treated at 450 °C in air for 4 h.[157] The electrochemical reduction was conducted under 40 V for 200 s in an ethylene glycol solution containing 0.27 wt% NH_4F after a brief activation treatment (typically, at 60 V for 30 s, or 4 V for 600 s).[157] Zhou and Zhang adopted similar strategy in making black TiO_2 nanotubes.[158] The pristine nanotubes were made by anodizing Ti foil in a Ti-platium two-electrode system under 20 V for 2 h as 25 °C in ethylene glycol containing 0.5 wt % NH_4F and 10 wt % H_2O, followed by annealing at 450 °C for 2 h.[158] Zheng prepared black TiO_2 films with a multipulse anodization method.[159] The fabricated TiO_2 films had tens of well-defined layers with long-range structural periodicity and photonic band gaps in the visible wavelengths.[159] The color was electrically switchable between green and black.[159]

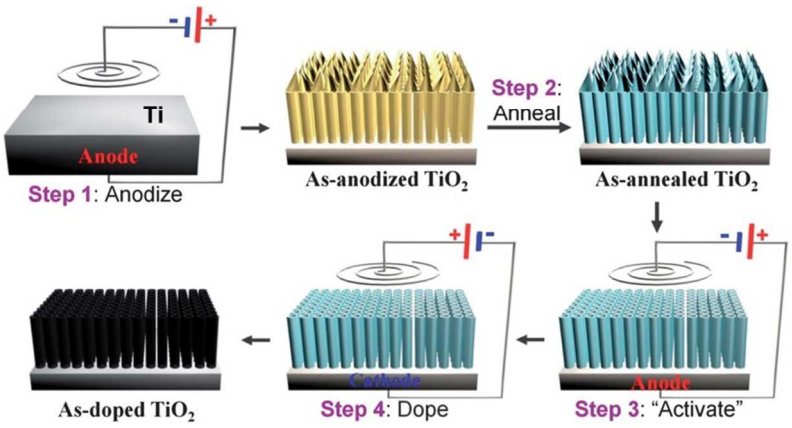

Figure 21. Illustration of the fabrication procedure for obtaining black TiO_2 nanotubes with electrochemical reduction method.[157] Reprinted with permission from ref 157. Copyright 2014, The Royal Society of Chemistry.

2.6 Anodization-Annealing

Dong et al prepared black TiO_2 nanotubes by anodization followed with annealing as shown in Figure 22.[160] TiO_2 nanotubes were first obtained after two 10 h anodization on a Ti foil at 60 V in ethylene glycol containing 0.25 wt.% NH_4F and 2 vol.% distilled water.[160] The TiO_2 nanotubes after the first anodization were removed before the second anodization.[160] The anodized Ti foil was cleaned in ethanol and distilled water, dried at 150 °C, and then sintered at 450 °C for 1 h in ambient atmosphere.[160] A layer of black TiO_2 was obtained on the substrate after removing the top oxide layer.[160]

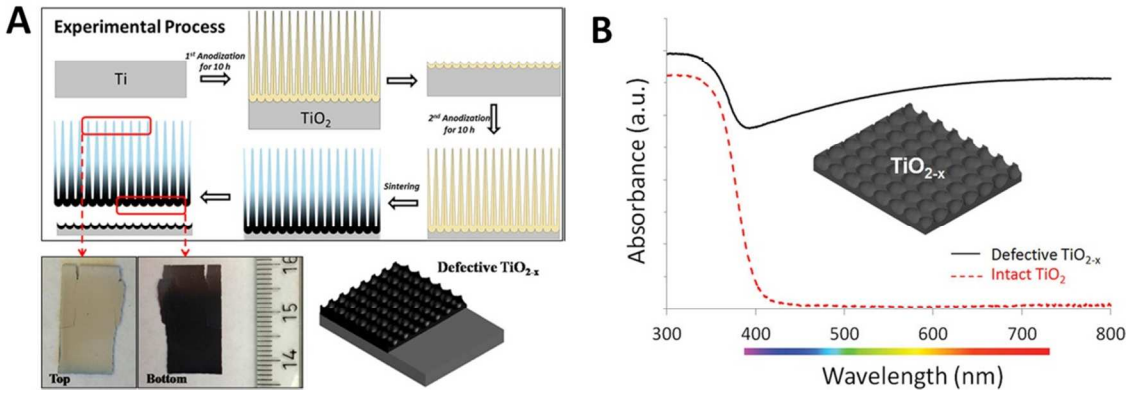

Figure 22. (A) Illustration of the experimental Process and images of the stripped TiO_2 nanotubes. (B) UV-visible absorption spectra of TiO_2 nanotubes.[160] Reprinted with permission from ref 160. Copyright 2014, American Chemical Society.

3. Properties of black TiO_2 nanomaterials

Since the fabrication methods and conditions of black TiO_2 nanomaterials in the literature vary one from the others, it is commonly reported that the various black TiO_2 nanomaterials displayed different chemical and physical properties, as briefly summarized in the following sections. Some of these properties, if not all, have been used to explain the black color of the reported TiO_2 nanomaterials.

3.1 The existence of structural disorder near the surface

Disordered structural features have been reported near the surface of black TiO_2 nanoparticles with a crystalline/disordered core/shell structure in some studies,[75,98,99,102,106,119,121,134,137,140] however, different observation has also been reported.[125] For examples, a disordered surface layer was observed surrounding the crystalline core by Chen, et al. in the hydrogenated black TiO_2 nanoparticles obtained

under 20 bar at 200 °C,[75,98,99] by Lu et al. in the hydrogenated TiO_2 nanocrystals obtained by treating the commercial Degussa P25 under 35 bar hydrogen and room temperature up to 20 days,[102] in the hydrogenated black TiO_2 nanosheets by Wang and Xu,[106] in hydrogenated TiO_2 nanocrystals by Naldoni, et al.,[119] in black TiO_2 nanoparticles by hydrogen plasma,[137] and in black TiO_2 nanocrystals obtained by reducing with aluminum by Wang et al.,[140] etc. Lattice contraction in the disordered layer was reported by some groups,[98,99,106,119] however, a weak lattice expansion was also suggested by the hydrogenation treatment.[114] On the other hand, Lu and Zhou, et al. found that the hydrogenated TiO_2 nanotubes had a very clear surface.[125]

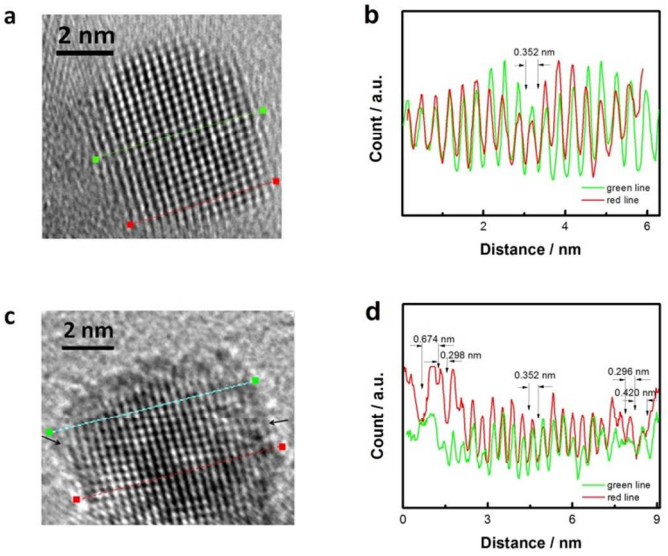

Figure 23. HRTEM (**a**) and line analyses (**b**) of one white TiO_2 nanoparticle, HRTEM (**c**) and line analyses (**d**) of one black TiO_2 nanoparticle. The zeros of the axis in **b** and **d** correspond to the left ends of the lines in **a** and **c**. The red, and green curves in **b** and **d** correspond to the red and green lines in **a** and **c.**[99] Reprinted with permission from ref 99. Copyright 2013, Nature Publishing Group.

High-resolution transmission electron microscopy (HRTEM) has been commonly used to differentiate the disordered phase from the crystallaine phase in the black TiO_2 nanoparticles.[75,98,99,102,106,119,121,137,140] For example, Figure 23 shows the HRTEM and line analysis of one normal white TiO_2 nanoparticle in comparison with one black TiO_2 nanoparticle.[99] The white TiO_2 nanoparticle displayed clearly-resolved and well-defined lattice fringes, even at the surface of the nanocrystal (Figure 23a), and the distance between the adjacent lattice planes was typical for anatase (0.352 nm) and uniform throughout the whole nanocrystal (Figure 23b).[99] The black TiO_2 nanoparticle had a crystalline-disordered core-shell structure (Figure 23c),[99] and a structural deviation from the standard crystalline anatase was readily seen at the outer layer, where the straight lattice line was bent at the edge of the nanoparticle, and the plane distance was no longer uniform (Figure 23d).[99] Sometimes, electron diffraction (ED) has also been used to identify the amorphous structure from the crystalline phase.[161] The nanoparticles containing only crystalline phase gave clear diffraction patterns made of diffraction dots or rings, but the nanoparticles having both crystalline and disordered phases produced cloudy diffraction patterns instead.[161] Fast Fourier transform (FFT) of the HRTEM images is also a useful technique to reveal the crystalline and amorphous structures in black TiO_2 nanoparticles.[119]

X-ray diffraction (XRD) is a commonly used technique to analyze crystalline phase structures in black TiO_2 nanoparticles;[75,102,106,119] however, it is a bulk analysis technique and only sensitive to the crystalline phase. In the XRD pattern, the diffraction peaks might shift to the higher diffraction angles in black TiO_2 nanoparticles, suggesting that the reduction of the interplanar distance of the crystalline phase.[98,106] Raman

spectroscopy has been used as a complimentary structural characterization to XRD in probe the amorphous or disordered structures in black TiO_2 nanoparticles.[75,106] In the Raman spectroscopy, the scattering peaks became much weaker in intensity,[75,106,121,124,125] broader in width,[102,110,119,124,129,134,136,140] shifted to higher wavenumbers,[101,110,113,119,124,129,140,141] and additional small vibrational modes were observed in black TiO_2 nanoparticles.[75,121,134,147] Both XRD and Raman techniques provide the assemble information of the overall properties. Combining XRD with HRTEM, estimation of the volumes and percentages of disordered phase over the crystalline phase in black TiO_2 nanoparticles has also been attempted.[98]

3.2 The existence of Ti^{3+} ions

Depending on the synthetic conditions of black TiO_2 nanomaterials, Ti^{3+} ions can be observed or not seen experimentally. In some black TiO_2 nanomaterials from hydrogen reduction or by hydrogen plasma, Ti^{3+} ions were not detected in hydrogenated black TiO_2 nanocrystals with conventional X-ray photoelectron spectroscopy (XPS),[75,117-119] synchrotron X-ray absorption, emission and photoelectron spectroscopies,[99] and electron spin resonance spectroscopy (ESR).[103,137,161,162] For example, Wang et al. found that suggested the absence of Ti^{3+} in the black hydrogenated TiO_2 nanowires treated at 450 °C based on the almost identical Ti 2*p* XPS spectra of pure and hydrogenated TiO_2 nanowires.[118] However, in some reports, the existence of Ti^{3+} ions in the black TiO_2 nanomaterials was found from hydrogen treatment,[106,113,115,119,121,125] chemical reduction,[141,142,146] chemical oxidation,[141,152] and electrochemical reduction.[155,160] For

example, Ti^{3+} ions were detected with XPS in the black TiO_2 nanotubes obtained by electrochemical reduction[156] and from the oxidation of TiH_2.[152]

3.3 The existence of oxygen vacancies

Oxygen vacancies have been constantly reported in black TiO_2 nanomaterials from with hydrogen thermal treatment,[106,111,116,118,121,163,164] electrochemical reduction,[152,165] chemical reduction[142,143,147] and chemical oxidation.[166] For example, oxygen vacancies were seen with ESR spectroscopy in the black TiO_2 nanoparticles from Al reduction,[142,143] in the black TiO_2 nanotubes from thermal hydrogen treatment[103,105] and electrochemical reduction.[160] However, in some cases, oxygen vacancies were not observed. For example, no oxygen vacancy was detected with ESR in the black TiO_2 nanoparticles prepared with thermal treatment in the studies by Xia, et al.[161,162]

3.4. The existence of Ti-OH groups

In the black TiO_2 nanomaterials treated with hydrogen, the OH content changed after the hydrogenation treatment. A shoulder peak of Ti–OH in the O 1*s* XPS spectrum was found in hydrogenated black TiO_2 nanoparticles treated at 200 °C for 5 d,[75] in the hydrogenated TiO_2 nanowires[118] and in the hydrogenated TiO_2 nanotubes with ultrahigh purity H_2 atmosphere at 200 – 600 °C for 1 h.[115,117] However, no change of Ti–OH in the O 1s spectra was observed in the hydrogenated TiO_2 nanotube arrays treated at 450 °C for 1 h in a reducing 5% H_2 and 95% Ar atmosphere,[125] and a decreased OH signal was observed in the O 1*s* XPS spectrum, for the hydrogenated black TiO_2 nanoparticles treated at 450 °C for 4 h under 5 bar H_2.[161,162]

In the Fourier transform infrared (FTIR) spectrum, the hydrogenated black TiO_2 nanomaterials showed the intensity change of the OH vibrational band.[99,106,125,134,137,161,162] More surface OH groups were observed on hydrogenated TiO_2 nanosheets treated at 400 °C for 2 h under a 10 bar pure H_2 atmosphere.[106] Hydrogenated TiO_2 nanoparticles treated by hydrogen plasma for at 500 °C 4 - 8 h displayed extra peaks at 3685, 3670, and 3645 cm^{-1} and at 3710 cm^{-1}.[137] In hydrogenated TiO_2 microspheres treated at 500 °C for 4 h under a flow of H_2 (5 % in N_2, 300 sccm), the intensity of the OH peak was much lower than pure TiO_2.[134] Less adsorbed water and/or hydroxyl groups was present in the hydrogenated TiO_2 nanotubes treated at 450 °C for 1 h in a reducing 5% H_2 and 95% Ar atmosphere based on the weaker bands at 3446 and 1645 cm^{-1}.[125] An decreased O–H intensity was observed for hydrogenated black TiO_2 treated at 200 C for 5 d,[99] and no OH absorption bands was found in hydrogenated TiO_2 nanocrystals treated at 450 °C for 4 h under 5 bar H_2.[161,162]

In the ^1H nuclear magnetic resonance (NMR) spectra, a higher peak at 5.5 ppm from bridging hydroxyl groups was observed in the hydrogenated TiO_2 nanocrystals groups treated by hydrogen plasma at 500 °C for 4 - 8 h, and extra signals at 0.01 and 0.4 ppm from the internal and terminal hydroxyl.[137] A slightly broader peak at chemical shift +5.7 ppm with two additional small and narrow peaks at chemical shifts -0.03 and 0.73 ppm was seen in the hydrogenated black TiO_2 nanocrystals treated at 200 °C for 5 d.[99] However, much smaller OH signals were found for the hydrogenated TiO_2 nanocrystals heated at 450 °C for 4 h under 5 bar H_2.[161,162]

3.5 The existence of Ti-H groups

The appearance of Ti-H groups was sometimes reported in hydrogenated black TiO_2 nanomaterials.[106,117,134,137] A shoulder peak around 457.3 eV in the Ti 2p XPS spectrum due to the surface Ti–H bonds was found in hydrogenated TiO_2 nanowire microspheres treated at 500 °C for 4 h under a flow of H_2 (5 % in N_2, 300 sccm)[134] and in the hydrogenated TiO_2 nanocrystals treated by hydrogen plasma at 500 °C for 4 - 8 h.[137] Ti–H bonds were suggested to cover the surface of hydrogenated TiO_2 nanosheets obtained at 400 °C for 2 h under 10-bar pure H_2 atmosphere.[106] The formation of Ti–H bond was also suggested from the diffraction peak at approximately 59.28° in the X-ray diffraction (XRD) pattern of hydrogenated TiO_2 nanotubes treated in ultrahigh purity H_2 atmosphere at 200 – 600 °C for 1 h.[117]

3.6 The modifications of the valence band edge

Shift in the valence band was sometimes observed in the black TiO_2 nanomaterials.[75,119,125,141,143,144,148,157,167] For example, a red shift of the valence band was observed from valence-band XPS spectrum for the hydrogenated TiO_2 nanoparticles treated at 200 C for 4 d under 20 bar H_2[75] or heated at 500 °C for 1 h under hydrogen atmosphere,[119] in the black brookite TiO_2 nanoparticles,[143] rutile TiO_2 nanoparticles,[144] and TiO_2 nanotubes[141] prepared with the Al reduction method, in the black anatase TiO_2 nanotubes by $NaBH_4$ reduction,[148] in the black TiO_2 nanoparticles by electron beam treatment,[167] in the hydrogenated TiO_2 nanotubes treated at 450 °C for 1 h in a reducing 5% H_2 and 95% Ar[125] and in the black TiO_2 nanotubes electrochemically hydrogenated.[157] Ti^{3+} ions was found not contribute to extra bandgap states of the hydrogenated TiO_2 nanocrystals,[99] as when Ti^{3+} showed up, the these midgap states disappeared.[99] On the

other hand, similar valence-band structures was seen for pure and hydrogenated TiO_2 nanowires treated with ultrahigh purity hydrogen atmosphere (ambient pressure) at 200 – 550 °C for 3 h.[118] Similar observations were reported on hydrogenated TiO_2 nanosheets as well.[106,137]

Table 1 summarizes the various black TiO_2 nanomaterials with different method and their properties. It is clearly seen that the structural, optical, chemical and electronic properties largely depends on the preparation methods and conditions. Thus it is important in our practice to pay attention to the experimental procedures and details in order to obtain the desired properties that we are targeting.

3.7 Theoretical consideration of hydrogenated black TiO_2 nanomaterials

First-principles calculations by Aschauer and Selloni suggested that hydrogen migration from anatase (101) surface to subsurface sites had smaller kinetic barriers than desorption.[171] The H adsorption energy at subsurface sites was about 0.4 eV smaller than at surface sites and was entropically favored.[171] Atomic hydrogen was likely to diffuse into the subsurface and further into the bulk, especially at higher coverage.[171] Subsurface vacancies were stable in reduced anatase and favorably accommodated hydrogen.[171] Highly reduced anatase enhanced hydrogen incorporation in the bulk.[171]

Periodic density functional theory calculations by Raghunath, et al. suggested that both H atoms and H_2 molecules migrated into TiO_2 near subsurface layer from TiO_2 (101) surface were equally favorable.[172] The dissociative adsorption of H_2 on the surface was the controlling step for H migration.[172] The presence of H atoms on the surface and inside the subsurface layer promoted both H and H_2 penetration into the subsurface layer, and

prevented the escape of the H_2 from the cage.[172] The H_2 molecule inside a cage readily dissociated and formed 2HO-species exothermically, which further transformed into H_2O and resulted in the formation of O-vacancies and surface disordering.[172] The interstitial H, H_2, and H_2O brought in density of states within the TiO_2 band gap and induced a shift of the band gap position notably towards the conduction band.[172]

In the study by Chen, et al.,[75] the H atoms were suggested to bond to O and Ti atoms.[75] Two groups of midgap states were predicted at about 3.0 and 1.8 eV, with the higher-energy group made of Ti 3d orbitals, and the lower-energy group mixed of O 2p and Ti 3d orbitals.[75] The hydrogen 1s orbital mainly passivated the dangling bonds and stabilized the lattice disorders, which contributed to the midgap states.[75] In the DFT-PBE calculations by Lu et al., hydrogen atoms were chemically absorbed both on Ti_{5c} and O_{2c} atoms for (101), (001), and (100) surfaces by taking into account the synergistic effect of Ti–H and O–H bonds.[168] The hydrogenation-induced lattice distortions on (101) and (100) surfaces of nanoparticles enhanced the intraband coupling within the valence band, while the (001) surface was not largely affected.[168] The adtoms not only induced the lattice disorders but also interacted strongly with the O 2*p* and Ti 3*d* states, resulting in a considerable contribution to the midgap states.[168] The optical absorption was dramatically redshifted due to the midgap states and the photogenerated electron–hole separation was substantially promoted as a result of electron–hole flow between different facets of hydrogenated nanoparticles.[168]

Liu, et al. later pointed out that hydrogenated black TiO_2 required not only hydrogen passivation of Ti and O dangling bonds on the surface.[100] The conduction band minimum (CBM) did not change upon the O distortion, redshifted upon the Ti-sublattice

distortion; the valence band maximum (VBM) blueshifted on either case.[100] The little effect of the O distortion upon CBM was attributed to the nature of Ti 3d orbital featured CBM.[100] The lattice disorder was mainly due to the O distortion.[100] Hydrogenation played an important role in reducing the distortion energy in raising the VBM.[75,100] The CBM electrons were not sensitive to local lattice distortions nor to H bonding induced changes.[100] The midgap states changed upon both lattice distortion and H bonding.[100] The lattice distortion caused by H in bulk anatase was not most stable and might release hydrogen from the lattice even at room temperature.[100]

Pan, et al. found H-doping had different effects on the electronic properties of three TiO_2 polymorphs - anatase, rutile, and brookite.[169] Although the incorporation of hydrogen was important for n-type TiO_2 formation, interstitial hydrogen caused bandgap narrowing, but substitutional hydrogen did not reduced bandgap of anatase.[169] (H, N)-co-doping narrowed the bandgap of anatase and brookite TiO_2, but had little effect on rutile TiO_2.[169] Based on density functional–pseudopotential calculations by Sotoudeh et al., O/Ti termination was the most stable surface on anatase (001) TiO_2, the valence band comes from p-states of deep and surface O atoms and d-orbitals of surface Ti atoms, and the conduction band comes from the d-orbitals of deep Ti atoms.[172] H doping injected electrons to clean (001) surface, created an empty mid-gap state below the conduction band and removed the mid-gap state in the (001) surface with O vacancy.[172]

Deng et al. found that real-hydrogen–passivated (RH-passivated) passivation of the nanostructured semiconductors could either increase or decrease the band gap, depending on the ionicity of the nanocompounds.[173] For anatase TiO_2, occupied gap states from the Ti-H bond with H s and Ti s and d characters were created at about 0.7 eV

above the host VBM and the effective band gap was reduced.[173] The position of occupied H-induced state (bonding cation-H state) near the VBM state was not affected much by the anion.[173] The first-principle calculations by Liu et al suggested that the absolute value of the O_2 adsorption energy was increased by H atoms on the anatase (101) surface or at subsurface sites.[174] The dissociation barriers of O_2 on an anatase surface were further decreased with two H atoms at the subsurface sites or with an H surface adatom and a subsurface atom.[174] After the dissociation, OH, H_2O, and O adatoms might form on the surface.[174]

4. Application examples of black TiO_2 nanomaterials

4.1 Photocatalysis

Before the report of hydrogenated black TiO_2 nanoparticles, hydrogen thermal treatment on TiO_2 has already been shown in enhancing its photocatalytic activities. Harris and Schumacher found that hydrogen reduction at high temperatures reduced recombination centers and increased the lifetime of the holes in the bulk TiO_2.[175] The improved photoactivity was likely due to the presence of oxygen vacancies, Ti^{3+} species, and hydroxyl groups induced by this treatment.[175] Heller, et al. found by treating it in H_2 at 550 °C the photoactivity of rutile TiO_2 was enhanced due to the increased E_F and the energy barrier which pushed electrons away from the surface.[176] Liu, et al. reported that anatase TiO_2 nanoparticles treated with H_2 at 500 – 600 °C had enhanced performance in sulfosalicylic acid's photodecomposition.[112]

Chen, et al. found that the hydrogenated black TiO_2 nanoparticles obtained by treating at 200 °C for 5 d under 20 bar H_2 had much higher photocatalytic activities in

decomposing organic pollutants (methylene blue and phenol) and generating H_2 from water/methanol solution.[75] Wang and Li, et al. reported that hydrogenated black TiO_2 nanowires treated under ultrahigh purity hydrogen atmosphere (ambient pressure) for 3 h at 200 – 550 °C displayed enhanced photoelectrochemical water-splitting performance.[118] Zheng, et al. found that hydrogenated black anatase nanowire microspheres prepared at 500 °C for 4 h under a flow of H_2 (5 % in N_2, 300 sccm) improved enhanced photocatalytic activity in photodecomposition of 2,4-dichlorophenol in the visible-light region.[134] Wang and Xu, et al. reported that hydrogenated black TiO_2 nanosheets obtained at 400 °C for 2 h under 10-bar pure H_2 atmosphere had an enhanced photocatalytic activity in decomposing methylene blue.[106] Wang and Jiang, et al. produced black TiO_2 under hydrogen plasma yielded large improvement in photocatalytic decomposition of methyl-orange.[137] Danon, et al. reported that the hydrogenated TiO_2 nanotubes under a flow of 5% H_2 in Ar at atmospheric pressure at 350 °C for 3 h had better photocatalytic activity in removing acetaldehyde under visible light.[127] Yu et al. demonstrated that by tuning the hydrogenation conditions (under a H_2 gas flow (50 sccm) at atmospheric pressure in a quartz tube at 500 – 700 °C for various time), the photocatalytic activity of hydrogenated TiO_2 nanocrystals in decomposing methylene blue under UV light was flexibly controlled through the control of the bulk to surface defect distribution.[113] Lu et al. showed hydrogenated TiO_2 nanocrystals by treating the commercial Degussa P25 under 35 bar hydrogen and room temperature up to 20 days, displayed improved photocatalytic activity in hydrogen generation.[102] Hoang found hydrogenation and nitridation on TiO_2 nanowires improved the visible-light performance in photo-oxidation of water.[131] However, Leshuk, et al. found that hydrogenated TiO_2

nanoparticles prepared at 200 °C under a 300±5 psig pure H_2 gas environment for 5 days or at 400 – 500 °C for 102 h under a 10% H_2 + 90% Ar gas flow showed worse photocatalytic activities in decomposing methylene blue than pure TiO_2 nanocrystals.[109,110]

Liu et al. compared the cocatalyst-free photocatalytic activities in generating hydrogen from water of hydrogenated TiO_2 nanotubes and nanorods treated under several conditions: (i) an anatase TiO_2 nanotube layer (air); (ii) this layer converted with Ar (Ar) or H_2/Ar (H_2/Ar); (iii) a high pressure H_2 treatment (20 bar, 500 °C for 1 h) (HP-H_2); and (iv) a high pressure H_2 treatment but mild heating (H_2, 20 bar, 200 °C for 5 d) (Sci ref).[103] They found that hydrogenated TiO_2 nanotubes from high pressure H_2 treatment had a high open circuit photocatalytic hydrogen production rate without the presence of a cocatalyst, in comparison to the nonactivity of those from atmospheric pressure H_2/Ar annealing and the hydrogenated rutile nanorods (Figure 24).[103] The high H_2 pressure annealing induced room-temperature stable, isolated Ti^{3+} defect-structure created in the anatase nanotubes.[103] They suggested that clearly an adequate H_2 treatment was needed to form these centers and the detailed experimental procedure seems to be crucial.[103] A considerable difference in reactivity existed on the hydrogenation conditions and the phase of the TiO_2 nanomaterials.[103]

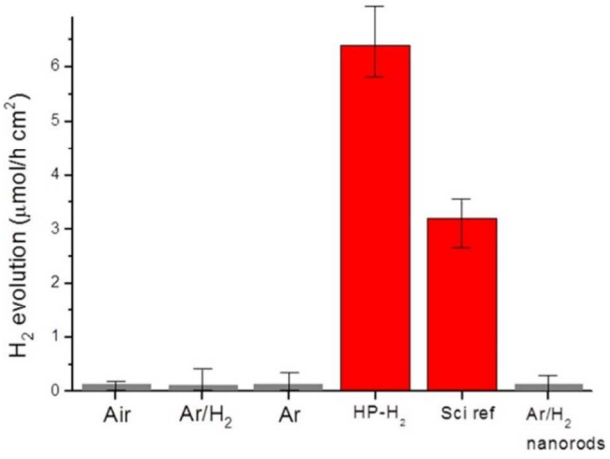

Figure 24. Photocatalytic H_2 production under open circuit conditions in methanol/water (50/50 vol %) with TiO_2 nanotubes and nanorods treated in different atmospheres under AM1.5 (100mW/cm^2) illumination.[103] Air, heat treatment in air at 450 °C; Ar, heat treatment in pure argon at 500 °C; Ar/H_2, heat treatment in H_2/Ar (5 vol %) at 500 °C; HP-H_2, heat treatment in H_2 at 20 bar at 500 °C; Sci ref, heat treatment in H_2 at 20 bar at 200 °C for 5 days (following ref 72).[103] Reprinted with permission from ref 103. Copyright 2014, American Chemical Society.

Xu et al.[155] and Zhang et al.[156] reported that electrochemically reduced black TiO_2 nanotubes obtained with an electrochemical reduction method showed improved performance in photoelectrochemical water splitting. Li et al. showed the electrochemically reduced black anatase TiO_2 nanotubes with a largely improved photocatalytic activity in decomposing Rhodamine.[157]

Wang et al. found that black anatase nanoparticles from Al reduction showed enhanced photocatalytic activity in decomposing methyl orange under both UV and visible-light irradiations.[140] More completely degradation of MO by Al-reduced TiO_2 suggests the high mineralization efficiency of black titania, revealing a improved

photooxidation.[140] Cui et al. demonstrated that black anatase TiO_2 nanotubes from Al reduction had improved photoelectrochemical water-splitting performance.[141] Yin et al. showed that gray anatase TiO_2 nanowires from Al reduction displayed higher photocatalytic activity in decomposing methyl orange under sunlight irradiation.[142] Zhu et al. showed that black brookite nanoparticles from Al reduction had enhanced photocatalytic activities in decomposing methyl orange and methylene blue under sunlight.[143] Yang et al. showed the black rutile TiO_2 nanoparticles from Al reduction with improved photoelectrochemical water-splitting performance under both UV and visible-light irradiations (Figure 25).[144] Lin et al. found that the black P25 nanoparticles with non-metal dopants had increased photocatalytic activity in hydrogen generation under both UV and visible-light irradiations.[145]

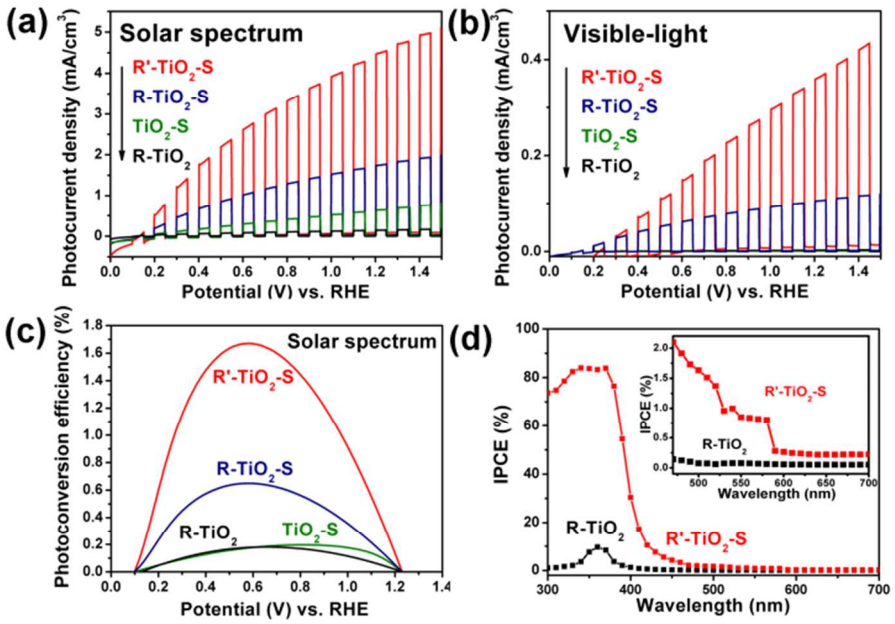

Figure 25. Photoelectrochemical properties of R'-TiO_2-S, R-TiO_2-S, TiO_2-S and R-TiO_2 electrodes: Chopped J-V curves (a) under simulated solar light illumination and (b) under visible-light illumination using three electrode setup (TiO_2 working, Pt counter, Ag/AgCl reference electrode, scan rate of 10 mV/s) in 1 M NaOH electrolyte (pH = 13.6); (c)

photoconversion efficiency as a function of applied potential; (d) IPCE spectra in the region of 300-700 nm at 0.65 V_{RHE}; Inset: IPCE spectra in the region of 420-700 nm.[144] Reprinted with permission from ref 144. Copyright 2013, American Chemical Society.

Zhao et al. reported that black rutile TiO_2 nanorods from Zn reduction had improved photocatalytic activity in producing hydrogen from water/methanol solution under both UV and visible-light irradiations.[146] Zou found gray TiO_2 nanoparticles by imidazole reduction improved photocatalytic activity in producing hydrogen from water/methanol solution under both UV and visible-light irradiations.[147] Kang showed enhanced photoelectrochemical performance of the black anatase TiO_2 nanotubes by $NaBH_4$ reduction.[148] Black TiO_2 nanoparticles from the oxidation of TiH_2 by H_2O_2 had enhanced photocatalytic activities in both methylene blue decomposition and hydrogen generation under visible-light irradiation by Liu et al. [151] and Grabstanowicz et al. [152]

Gallo et al. reported that Pt-Au nanoparticles supported on reduced anatase TiO_2 nanocrystals showed remarkable photocatalytic activity in generating hydrogen from water/ethanol or water/glycerol solutions under both UV and simulated sunlight irradiations.[177,178] The Pt-Au nanoparticles were loaded on the TiO_2 nanoparticle surface with an impregnation method with $(NH_4)_2PtCl_6$ and $HAuCl_4$ solutions, followed by heating in flow O_2 gas at 200 °C for 1 h. The hydrogen reduction was conducted in flow H_2 gas at 250 or 500 °C for 1 h.[177,178] The good photocatalytic activity was attributed to the presence of bimetallic Pt–Au nanoparticles, Ti^{3+} sites/O^{2-} vacancies in the bulk, for maximizing light absorption and feedstock activation.[177,178]

The enhanced photocatalytic and photoelectrochemical activities of black TiO_2 nanomaterials have been frequently attributed to the existence of more oxygen vacancies,[118,140-148,151] Ti^{3+} ions,[140-145,151,153] surface Ti-OH groups,[75,118] surface Ti-H groups,[75,117,134] narrower bandgap,[134] better charge separation[140-145] and possibly the combination of these species.[140-145,151] These reasons have also been adopted for pure or doped TiO_2 nanomaterials as well.[179-186] For example, Wang attributed the enhanced photocatalytic activity of {001}-facets-dominated anatase TiO_2 nanosheets to the existence of oxygen vacancies and Ti^{3+} defects from the hydrothermal reaction.[179] Pan et al. found TiO_2 nanoparticles with oxygen vacancies has been reported to spontaneously reduce gold or Pd on the surface and to have enhanced visible light photoactivity toward Rhodamine B (RhB) degradation or reduction of nitroaromatics.[180,181] Kong found that decreasing the relative concentration ratio of bulk defects to surface defects in TiO_2 nanocrystals significantly improved the separation efficiency of photogenerated electrons and holes and the photocatalytic efficiency.[182]

4.2 Photoelectrochemical sensor

Zhang et al. reported hydrogenated black TiO_2 nanorods as a photoelectrochemical sensor for organic compounds under visible light.[118] The hydrogenated TiO_2 nanorods were obtained by treating TiO_2 nanorods in H_2/Ar flow (20:80 sccm) at 350 °C for 1 h under ambient pressure.[118] The starting TiO_2 nanorods were prepared on a fluorine-doped tin oxide (FTO) glass slide by reacting titanium butoxide (0.48 mL) in HCl solution (40 mL 18.25 wt%) at 170 °C for 6 h.[118] Under UV and visible light, the hydrogenated TiO_2 nanorods showed a highly sensitive and steady

photocurrent response on several organic compounds: glucose, malonic acid and potassium hydrogen phthalate (Figure 26), due to introduction of oxygen vacancy and mid-gap energy levels.[118] The increase of the photocurrent was suggested mainly due to the improvement of electronic conductivity that resulted from the creation of mid-energy levels, rather than the enhancement in the UV and visible-light absorption after the hydrogenation process.[118] The improved electrical conductivity was beneficial to the separation of electron–hole pairs and electron collection from the oxidation of water and organic compounds.[118]

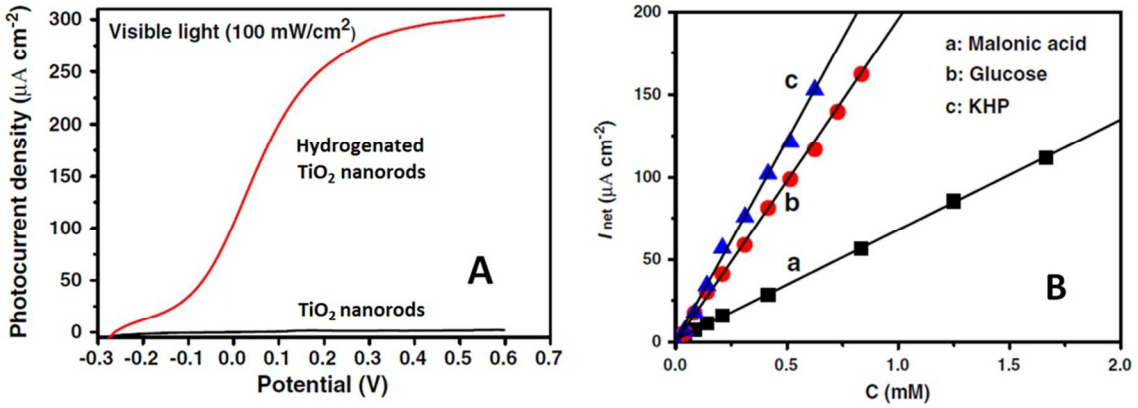

Figure 26. (A) The voltammograms of TiO_2 nanorods and hydrogenated TiO_2 nanorods obtained at a scan rate of 5 mV/s under visible light irradiation, (B) Relationships between I_{net} and concentrations of various organic compounds. KHP: potassium hydrogen phthalate.[118] Reprinted with permission from ref 118. Copyright 2014, Elsevier.

4.3 Catalysis

Barzan et al recently reported that reduced in hydrogen reduced TiO_2 displayed excellent catalytic activity in the conversion of ethylene to high density polyethylene (HDPE) under mild conditions (room temperature, low pressure, absence of any

activator).[120] The hydrogenation reaction was conducted under pure hydrogen atmosphere (pressure of 200 mbar) at 500 °C for 1 h.[120] Upon H_2 reduction, a broad and featureless absorption appears throughout the whole visible, near infrared, and mid infrared regions due to the creation of shallow-trapped defect sites (Ti^{4-n} and oxygen vacancies).[120] Their UV-visible and infrared spectroscopic studies of the reaction process suggested that ethylene polymerization occurred on the Ti^{4-n} defect sites in the reduced TiO_2 nanoparticles.[120] The defects behaved as shallow-trap defects located in the band gap.[120] These results opened valuable new applications for TiO_2 nanomaterials as catalysts.[120]

Zeng et al. reported that hydrogenated TiO_2 nanoparticles could decompose gaseous formaldehyde without light irradiation at room temperature.[128] On the other hand, pure TiO_2 nanoparticles did not show good activity in decompositing gaseous formaldehyde without light irradiation at room temperature.[128] The hydrogenation was carried out under a flow of H_2/Ar mixture at 300 °C for 2 h.[128] The oxygen vacancies induced by hydrogenation was believed to be responsible for the catalytic activities of the hydrogenated TiO_2 nanoparticles in the dark.[128]

4.4 Lithium-ion rechargeable battery

TiO_2 has been suggested as a safer lithium-ion battery anode material over graphite, since the insertion/extraction of lithium proceeds within 1.5 – 1.8 V vs the Li^+/Li redox couple in TiO_2.[187-190] It has a theoretical capacity value of 335 $mAhg^{-1}$.[187,188] Shin, et al. reported that hydrogenated black TiO_2 nanocrystals treated at 450 °C for 1−7 h under a 5% H_2/ 95% Ar gas flow displayed excellent rate performance for lithium storage.[123] The high performance was attributed to the well-balanced Li^+/e^- diffusion in

the hydrogenated TiO_2 nanocrystals from the oxygen vacancies and increased electronic conductivity induced by the hydrogen reduction reaction.[123] Lu et al. reported that substantially improved high-rate performance was obtained by annealing anodized TiO_2 nanotubes or rutile nanowires at 450 °C for 1 h in a 5% H_2 and 95% Ar atmosphere (100 sccm flow rate) from the increase of electronic conductivity induced by a large number of oxygen vacancies produced from the hydrogenation treatment.[125] Shen, et al. found that by introducing Ti^{3+} through hydrogenation for higher electrical conductivity hydrogenated $Li_4Ti_5O_{12}$ nanowires treated at 500–700 °C for 1.5 h in 5% v/v H_2/Ar had high capacity (173 $mAhg^{-1}$ at C/5), excellent rate performance (121 $mAhg^{-1}$ at 30 C), and good stability.[126] Li, et al. found that hydrogenated mesoporous TiO_2 microspheres proceeded under ambient hydrogen pressure at 400 °C for 1 h showed twice the rate capability of mesoporous TiO_2 microspheres due to the combination of the short lithium-ion diffusion path and the high electronic conductivity.[114] Improved lithium battery performance in the hydrogenated TiO_2 nanocrystals was reported by Xia, et al. as well by heating TiO_2 nanoparticles at 200 °C for 5 d under 20 bar H_2.[191] The suggested reasons for the improved performance was attributed to reduced charge diffusion resistance within the disordered TiO_2 lattice in the hydrogenated TiO_2 nanoparticles.[191]

Myung et al. found that nanostructured black TiO_2 had a superior performance with a capacity of 127 $mAhg^{-1}$ at 100 C (20 A g^{-1}) and approximately 86% retention after 100 cycles at 25 °C (Figure 27).[136] The black TiO_2 nanoparticles were obtained by annealing a yellow TiO_2 gel in Ar gas at 400 – 600 °C for 5 h.[136] The white TiO_2 nanoparticles were obtained by annealing the gel in air.[136] The TiO_2 gel was obtained by stirring high-purity $TiCl_4$ dropwise to a distilled water-ethanol mixture with HF and urea

at 0 °C for 4 h, and then evaporating the solution slowly at 80 °C.[136] Yang et al. reported hydrogenated anatase TiO_2 nanoparticles prepared by a H_2 plasma treatment had a fast lithium storage performance due to the enhanced contribution of pseudocapacitive lithium storage on the particle surface, possibly from the combined effect of the disordered surface layers and Ti^{3+} species of H-TiO_2.[139]

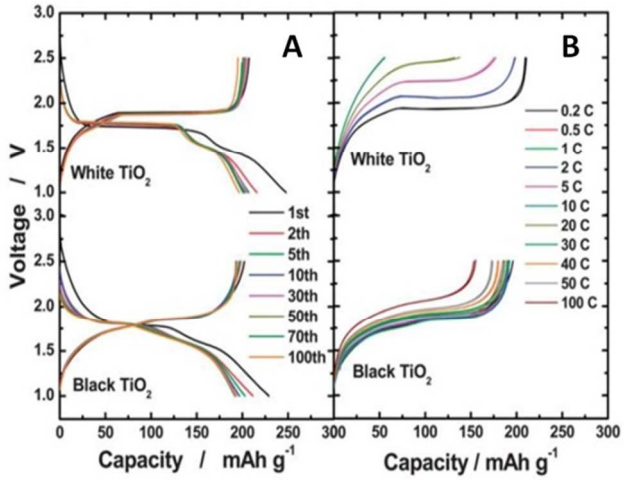

Figure 27. (A) Comparison of the continuous charge (Li^+ insertion) and discharge (Li^+ extraction) curves and (B) rate capability for the white and black anatase TiO_2 nanoparticles.[136] Reprinted with permission from ref 136. Copyright 2013, The Royal Society of Chemistry.

The suggested explanations for the enhanced performance as electrode materials in lithium-ion rechargeable batteries of the black TiO_2 nanomaterials included the creation of oxygen vacancies,[123,125] the existence of Ti^{3+} ions,[126] the well-balanced Li^+/e^- diffusion in the hydrogenated TiO_2 nanocrystals,[123] the increased electronic conductivity,[114,123,125,126] short lithium-ion diffusion path,[114] reduced charge diffusion resistance,[191] and pseudocapacitive lithium storage on the disordered particle surface.[136]

4.5 Supercapacitor

Lu et al. reported that hydrogenated black TiO_2 nanotube arrays obtained by heating anodized TiO_2 nanotubes under hydrogen environment between 300 to 600 °C displayed improved performance as supercapacitors due to increased densities of carrier and hydroxyl groups on TiO_2 surface from the hydrogenation.[115] When scanned at a rate of 100 mVs^{-1}, the hydrogenated TiO_2 nanotubes had a capacitance of 3.24 mF cm^{-2}, 40 times better than the air-annealed sample.[115] They showed 68% capacitance retention when the scan rate increased from 10 to 1000 mVs^{-1}, and had a good long-term cyclic stability (96.9% capacitance retention after 10000 cycles).[115] Li et al. also found that black anatase TiO_2 nanotubes from electrochemical reduction displayed much higher performance as a supercapacitor electrode, possibly due to their high conductivities.[157] In summary, the increased performance as electrode materials in supercapacitors of the black TiO_2 nanomaterials was suggested due to increased densities of charge carrier and hydroxyl groups on TiO_2 surface,[115] and the higher electrical conductivity.[157]

4.6 Fuel cell

Zhang, et al. reported that hydrogenated black TiO_2 nanotube obtained by annealing the anatase TiO_2 nanotubes in ultrahigh purity H_2 atmosphere at 200 – 600 °C for 1 h significantly improved fuel cells' performance and durability.[117] Their electrical conductivity (1.7 $mScm^{-1}$) increased 10 times and the increased numbers of oxygen vacancies and hydroxyl groups from hydrogenation for uniformly depositing a greater number of Pt nanoparticles.[117] The hydrogenation reduced the decrease in the

electrochemical surface area.[117] When used as anode in fuel-cell testing, they delivered a maximum power density of 500 $mWcm^{-2}$, and gave a specific power density of 2.68 $kWgPt^{-1}$ when loaded with Pt and used as the cathode.[117] The increased performance as electrode materials in fuel cells of the hydrogenated TiO_2 nanotube was suggested due to the increased electrical conductivity, oxygen vacancies, surface hydroxyl groups, and more uniform deposited Pt nanoparticles.[117]

4.7 Field Emission

Hydrogenated black TiO_2 nanotube arrays treated under a continuous hydrogen (8 sccm) and argon (10 sccm) flux for 5 h at 400 – 600 °C displayed a dramatically improved performance in field emission due to the increased conductivity and decreased work function.[124] Hydrogenation treatment reduced the turn-on field from 18.23 to 1.75 $V\mu m^{-1}$.[124] Black TiO_2 nanotube hydrogenated at 550 °C showed a low turn-on field, a high current density (4.0 mA cm^{-2} at 4.50 V μm^{-1}), and an excellent field emission stability over 480 min.[124] The substantially enhanced field emission properties was attributed to the a reduced work function and the improved conductivity.[124] Hydrogenation created oxygen vacancies as electron donors and increased the donor density of TiO_2.[124] The introduced oxygen vacancy states lifted the Fermi level and reduced the work function to decrease the field-penetration barrier at the surface resulting in easy electron emission.[124] Meanwhile, the oxygen vacancies from hydrogenation improved the electrical conductivity and charge mobility, and injected electrons transport easily to emission sites.[124]

4.8 Microwave absorption

Xia, et al. showed that hydrogenated TiO_2 nanocrystals displayed excellent microwave absorption performance, although TiO_2 is traditionally a good microwave absorption material, due to its low absorption in the gigahertz region.[163,164] Complex permittivity and permeability values are used to evaluate the microwave absorption properties.[163,164] The real and imaginary part of permittivity, ε' and ε", are related to the stored and dissipated electrical energy within the medium. Their ratio, $tg\delta_\varepsilon = \varepsilon"/\varepsilon'$, is called the dielectric dissipation factor, indicates the ratio of the lost electrical energy over stored.[163,164] Similarly, the real and imaginary part of permeability, μ' and μ", are related to the stored and dissipated magnetic energy within the medium. Their ratio, $tg\delta_\mu = \mu"/\mu'$, is called the dielectric dissipation factor, indicates the ratio of the lost magnetic energy over stored.[163,164] The hydrogenated TiO_2 nanocrystals/epoxy composites displayed larger ε' values in the frequency range 1.0–18.0 GHz with the average value about 4.3 times of the pure TiO_2 nanocrystals.[163,164] The ε" value (5.9 – 10.6) was around 70 larger than that of TiO_2 nanocrystals/epoxy composites (0.03–0.3),[163,164] and the $tg\delta_\varepsilon$ value was 15 times bigger.[163,164] The μ' and μ" values were slightly changed.[163,164] The hydrogenated TiO_2 nanoparticles had much stronger microwave absorption property than pristine TiO_2 nanoparticles.[163,164] A material with a reflection loss (RL) value less than -30 is regarded as an excellent absorber.[164] Apparently, hydrogenated TiO_2 nanoparticles had excellent microwave absorption performance (Figure 28A).[164] Figure 28B shows the simulations of the power reflection ratio of the pristine and hydrogenated TiO_2 nanoparticles.[164] Apparently, pristine TiO_2 nanoparticles didn't display much microwave absorption, while

all the hydrogenated TiO_2 nanoparticles had 99.9% reflection loss in certain microwave frequency ranges.[164]

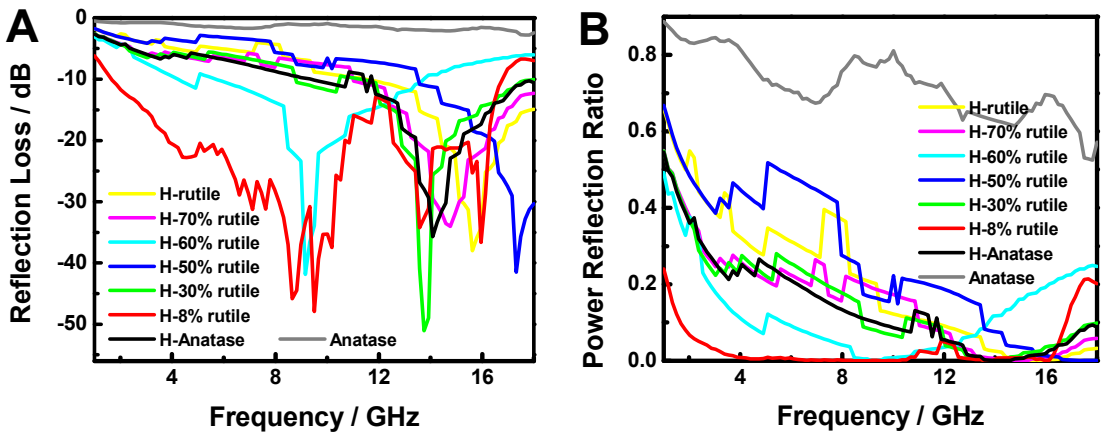

Figure 28. (A) reflection loss and (B) power reflection ratio of pristine and hydrogenated TiO_2 nanocrystals with various rutile compositions.[164] Reprinted with permission from ref 164. Copyright 2014, Materials Research Society.

5. Summary and prospective

Various synthetic methods: hydrogen thermal treatment, hydrogen plasma, chemical reduction, chemical oxidation, and electrochemical reduction have been developed to make black TiO_2 nanomaterials with various sizes, shapes, and morphologies. These different synthetic methods and conditions directly determine the various properties and performances of black TiO_2 nanomaterials originated from different research groups and published literatures. Black TiO_2 nanomaterials apparently have demonstrated excellent optical, chemical and electronic properties. These modified properties have been explained with either structural or chemical alterations or both in the black TiO_2 nanomaterials compared to white TiO_2 nanomaterials, such as lattice disorder near the surface layer, oxygen vacancies, Ti^{3+} ions, Ti-OH and Ti-H groups. These

various explanations are the natural extensions from the difference in the synthetic approaches and chemistries involved for black TiO_2 nanomaterials. Black TiO_2 nanomaterials have shown superior performance in photocatalysis and lithium-ion battery over white TiO_2 nanomaterials, and have also opened new applications with promising prospect in supercapacitors, fuel cells, photoelectrochemical sensors, field emission electrodes, and microwave absorbers. However, their activities in the visible-light region are still far from satisfactory, although black TiO_2 nanomaterials have shown large capabilities in absorbing a large amount of sunlight and have been sometimes reported with visible-light photocatalytic and photoelectrochemical activities. Managing the amount and spatial distributions of the sources of the blackness in the black TiO_2 nanomaterials, such as surface lattice disorder, oxygen vacancies, Ti^{3+} ions, Ti-OH and Ti-H groups, may also provide new opportunities and higher performance. Other possible reasons include that the black color only tells us the optical bandgap or the difference of the CBM and VBM and there is likely a mismatch between the electronic structures of the black TiO_2 nanomaterials and the photocatalytic and photoelectrochemical reactions we target for. Thus adjusting these potential matches either from materials point of views or chemical reactions may provide new opportunities in efficiently utilize the large amount of light being absorbed by these black TiO_2 nanomaterials, especially in the visible-light region. Apparently, more efforts are needed from synthesis to property and application in order to finally improve the efficiency of black TiO_2 nanomaterials for practical applications in renewable energy, environment and others.

6. Acknowledgements

X. C. thanks the support from the College of Arts and Sciences, the University of Missouri – Kansas City and the University of Missouri Research Board. L. L. acknowledges the support of the 100 Talents Program of the Chinese Academy of Sciences. F. H. thanks the support from National Science Foundation of China (Grant Nos. 51125006, 91122034, 51121064).

7. References

1. A. Fujishima and K. Honda, 1972. *Nature* **238**, 37.
2. A. J. Nozik *Nature* 1975, **257**, 383.
3. E. Borgarello, J. Kiwi, E. Pelizzetti, M. Visca and M. Grätzel *Nature* 1981, **289**, 158.
4. M. R. Hoffmann, S. T. Martin, W. Choi and D. W. Bahnemann, *Chem. Rev.* 1995, **95**, 69.
5. A. L. Linsebigler, G. Lu and J. T. Yates, *Chem. Rev.* 1995, 95, 735.
6. U. Diebold, *Surf. Sci. Rep.* 2003, **48**, 53.
7. X. Chen, S. Shen, L. Guo and S. S. Mao, *Chem. Rev.*, 2010, **110**, 6503.
8. X. Chen and S. S. Mao, *Chem. Rev.*, 2007, **107**, 2891.
9. L. Liu and X. Chen, *Chem. Rev.*, 2014, **114**, 9890.
10. C.-H. Lin, J.-H. Chao, Ch.-H. Liu, J.-C. Chang and F.-C. Wang, *Langmuir*, 2008, **24**, 9907.
11. H.-L. Kuo, C.-Y. Kuo, C.-H. Liu, J.-H. Chao and C.-H. Lin, *Catal. Lett.* 2007, **113**, 7.

12. C.-H. Lin, C.-H. Lee, J.-H. Chao, C.-Y. Kuo, Y.-C. Cheng, W.-N. Huang, H.-W. Chang, Y.-M. Huang and M.-K. Shih, *Catal Lett.* 2004, **98**, 61.

13. Y. Ma, X. Wang, Y. Jia, X. Chen, H. Han and C. Li, *Chem. Rev.*, 2014, **114**, 9987.

14. X. Chen, C. Li, M. Grätzel, R. Kostecki and S. S. Mao, *Chem. Soc. Rev.* 2012, **41**, 7909.

15. X. Chen and C. Burda, *J. Am. Chem. Soc.,* 2008*,* **130**, 5018.

16. W. Choi, A. Termin and M. R. Hoffmann, *J. Phys. Chem.* 1994, **98**, 13669.

17. W. Choi, A. Termin and M. R. Hoffmann, *Angew. Chem.* 1994, **106**, 1148.

18. N. J. Peill, L. Bourne and M. R. Hoffmann, *J. Photochem. Photobiol., A* 1997, **108**, 221.

19. S. T. Martin, C. L. Morrison and M. R. Hoffmann, *J. Phys. Chem.* 1994, **98**, 13695.

20. Y. Wang, Y. Hao, H. Cheng, H. Ma, B. Xu, W. Li and S. Cai, *J. Mater. Sci.* 1999, **34**, 2773.

21. H. Yamashita, Y. Ichihashi, M. Takeuchi, S. Kishiguchi and M. Anpo, *J. Synchrotron Radiat.* 1999, **6**, 451.

22. Y. Wang, H. Cheng, Y. Hao, J. Ma, W. Li and S. Cai, *J. Mater. Sci.* 1999, **34**, 3721.

23. A. Szabo and A. Urda, *Prog. Catal.* 2002, **11**, 73.

24. F. Coloma, F. Marquez, C. H. Rochester and J. A. Anderson, *Phys. Chem. Chem. Phys.* 2000, **2**, 5320.

25. M. Anpo, *Pure Appl. Chem.* 2000, **72**, 1265.

26. M. Anpo, *Pure Appl. Chem.* 2000, ***72***, 1787.

27. M. Anpo and M. Takeuchi, *Int. J. Photoenergy* 2001, **3**, 89.

28. M. Anpo, S. Kishiguchi, Y. Ichihashi, M. Takeuchi, H. Yamashita, K. Ikeue, B. Morin, A. Davidson and M. Che, *Res. Chem. Intermed.* 2001, **27**, 459.

29. M. Anpo and M. Takeuchi, *J. Catal.* 2003, **216**, 505.

30. C. Y. Wang, D. W. Bahnemann and J. K. Dohrmann, *Chem. Commun.* 2000, 1539.

31. W. Li, Y. Wang, H. Lin, S. I. Shah, C. P. Huang, D. J. Doren, S. A. Rykov, J. G. Chen and M. A. Barteau, *Appl. Phys. Lett.* 2003, **83**, 4143.

32. T. Mikulas, Z. Fang, J. L. Gole, M. G. White and D. A. Dixon, *Chem. Phys. Lett.* 2012, **539–540**, 58.

33. B. Liu, H. M. Chen, C. Liu, S. C. Andrews, C. Hahn and P. Yang, *J. Am. Chem. Soc.* 2013, **135**, 9995.

34. K. G. Roberts, M. Varela, S. Rashkeev, S. T. Pantelides, S. J. Pennycook and K. M. Krishnan, *Phys. Rev. B* 2008, **78**, 014409.

35. F. M. Dukes, E. Iuppa, B. Meyer and M. J. Shultz, *Langmuir* 2012, **28**, 16933.

36. H. A. Hamedani, N. K. Allam, H. Garmestani and M. A. El-Sayed, *J. Phys. Chem. C* 2011, **115**, 13480.

37. S. N. R. Inturi, T. Boningari, M. Suidan and P. G. Smirniotis, *J. Phys. Chem. C* 2014, **118**, 231.

38. R. Ghosh, Y. Hara, L. Alibabaei, K. Hanson, S. Rangan, R. Bartynski, T. J. Meyer and R. Lopez, *ACS Appl. Mater. Interfaces* 2012, **4**, 4566.

39. A. Ali, E. Yassitepe, I. Ruzybayev, S. I. Shah and A. S. Bhatti, *J. Appl. Phys.* 2012, **112**, 113505.

40. R. Asahi, T. Morikawa, T. Ohwaki, K. Aoki and Y. Taga, *Science* 2001, **293**, 269.

41. S. U. M. Khan, M. Al-Shahry and W. B., Ingler, Jr. *Science* 2002, **297**, 2243.

42. C. Burda, Y. Lou, X. Chen, A. C. S. Samia, J. Stout and J. L. Gole, *Nano Lett.* 2003, **3**, 1049.

43. X. Chen and C. Burda, *J. Phys. Chem. B* 2004, **108**, 15446.

44. T. Umebayashi, T. Yamaki, S. Yamamoto, A. Miyashita, S. Tanaka, T. Sumita and K. Asai, *J. Appl. Phys.* 2003, **93**, 5156.

45. T. Umebayashi, T. Yamaki, H. Itoh and K. Asai, *Appl. Phys. Lett.* 2002, **81**, 454.

46. H. Irie, Y. Watanabe and K. Hashimoto, *J. Phys. Chem. B* 2003, **107**, 5483.

47. T. Lindgren, J. M. Mwabora, E. Avendano, J. Jonsson, A. Hoel, C. G. Granqvist and S. E. Lindquist, *J. Phys. Chem. B* 2003, **107**, 5709.

48. H. Luo, T. Takata, Y. Lee, J. Zhao, K. Domen and Y. Yan, *Chem. Mater.* 2004, **16**, 846.

49. D. Li, H. Haneda, S. Hishita, N. Ohashi and N. K. Labhsetwar, *J. Fluorine Chem.* 2005, **126**, 69.

50. T. Ohno, M. Akiyoshi, T. Umebayashi, K. Asai, T. Mitsui and M. Matsumura, *Appl. Catal. A* 2004, **265**, 115.

51. T. Lindgren, J. Lu, A. Hoel, C. G. Granqvist, G. R. Torres and S. E. Lindquist, *Sol. Energy Mater. Sol. Cells* 2004, **84**, 145.

52. Y. Choi, T. Umebayashi and M. Yoshikawa, *J. Mater. Sci.* 2004, **39**, 1837.

53. D. Li, H. Haneda, N. K. Labhsetwar, S. Hishita and N. Ohashi, *Chem. Phys. Lett.* 2005, **401**, 579.

54. C. Di Valentin, G. Pacchioni and A. Selloni, *Phys. Rev. B* 2004, **70**, 085116/1.

55. C. Di Valentin, G. Pacchioni, A. Selloni, S. Livraghi and E. Giamello, *J. Phys. Chem. B* 2005, **109**, 11414.

56. C. Di Valentin, G. Pacchioni and A. Selloni, *Chem. Mater.* 2005, **17**, 6656.

57. D. Li, H. Haneda, S. Hishita and N. Ohashi, *Chem. Mater.* 2005, **17**, 2596.

58. Y. Kuroda, T. Mori, K. Yagi, N. Makihata, Y. Kawahara, M. Nagao and S. Kittaka, *Langmuir* 2005, **21**, 8026.

59. X. Chen, Y. Lou, A. C. S. Samia, C. Burda and J. L. Gole, *Ad*v. *Funct. Mater.* 2005, **15**, 41.

60. Z. Lin, A. Orlov, R. M. Lambert and M. C. Payne, *J. Phys. Chem. B* 2005, **109**, 20948.

61. J. Yuan, M. Chen, J. Shi and W. Shangguan, *Int. J. Hydrogen Energy* 2006, **31**, 1326.

62. S. Hoang, S. Guo, N. T. Hahn, A. J. Bard and C. B. Mullins, *Nano Lett.*, 2012, **12**, 26.

63. V. Likodimos, C. Han, M. Pelaez, A. G. Kontos, G. Liu, D. Zhu, S. Liao, A. A. de la Cruz, K. O'Shea, P. S. M. Dunlop, J. A. Byrne, D. D. Dionysiou and P. Falaras, *Ind. Eng. Chem. Res.* 2013, **52**, 13957.

64. J. W.J. Hamilton, A. Byrne, P. S.M. Dunlop, D. D. Dionysiou, M. Pelaez, K. O'Shea, D. Synnott and S. C. Pillai, *J. Phys. Chem. C* 2014, **118**, 12206.

65. G. Liu, C. Han, M. Pelaez, D. Zhu, S. Liao, V. Likodimos, A. G. Kontos, P. Falaras, D. D. Dionysiou, *J. Mol. Catal. A* 2013, **372**, 58.

66. J. Wang, D. N. Tafen, J. P. Lewis, Z. Hong, A. Manivannan, M. Zhi, M. Li and N. Wu, *J. Am. Chem. Soc.* 2009, **131**, 12290.

67. Q. Zhang, T. Gao, J. M. Andino and Y. Li, *Appl. Catal. B* 2012, **123– 124**, 257.

68. J. Zhang, J. Xi and Z. Ji, *J. Mater. Chem.* 2012, **22**, 17700.

69. H. Zhang , Y. Liang, X. Wu and H. Zheng, *Mater. Res. Bull.* 2012, **47**, 2188.

70. X. Wu, S. Yin, Q. Dong, C. Guo, T. Kimura, J.-i. Matsushita and T. Sato, *J. Phys. Chem. C*, 2013, **117**, 8345.

71. C. Yan, W. Yi, H. Yuan, X. Wu and F. Li, *Environ. Prog. Sust. Energy* 2014, **33**, 419–429.

72. M. Zhang, J. Wu, J. Hou and J. Yang, *Sci. Adv. Mater.* 2013, **5**, 535.

73. J. Jaćimović, R. Gaál, A. Magrez, L. Forró, M. Regmi and G. Eres, *Appl. Phys. Lett.* 2013, **102**, 172108.

74. Y. Sakatani, H. Ando, K. Okusako, H. Koike, J. Nunoshige, T. Takata, J. N. Kondo, M. Hara and K. Domen, *J. Mater. Res.* 2004, **19**, 2100.

75. X. Chen, L. Liu, P. Y. Yu and S. S. Mao, *Science* 2011, **331**, 746.

76. Y. H. Hu, *Angew. Chem. Int. Ed.* 2012, **51**, 12410

77. J. Qiu, J. Dawood and S. Zhang, *Chin. Sci. Bull.* 2014, **59**, 2144.

78. J. Buha, *J. Phys. D*. 2012, **45**, 385305.

79. H. G. Yang, C. H. Sun, S. Z. Qiao, J. Zou, G. Liu, S. C. Smith, H. M. Cheng and G. Q. Lu, *Nature*, 2008, **453**, 638.

80. A. Vittadini, M. Casarin and A. Selloni, *Theor. Chem. Acc.* 2007, **117**, 663.

81. C. Burda, X. Chen, R. Narayanan and M. A. El-Sayed, *Chem. Rev.* 2005, **105**, 1025.

82. D. C. Cronemeyer and M. A. Gilleo, *Phys. Rev.* 1951, **82**, 975.

83. D. C. Cronemeyer, *Phys. Rev.* 1952, **87**, 876.

84. R. G. Breckenridge and W. R. Hosler, *Phys. Rev.* 1953, **91**, 793.

85. D. C. Cronemeyer, *Phys. Rev.* 1959, **113**, 1222.

86. J. H. Becker and W. R. Hosler, *Phys. Rev.* 1965, **137**, 1872.

87. W. J. Lo, Y. W. Chung and G. A. Somorjai, *Surf. Sci.* 1978, **71**, 199.

88. V. E. Henrich and R. L. Kurtz, *Phys. Rev.* 1981, **23**, 6280.

89. M. S. Lazarus and T. K. Sham, *Chem. Phys. Lett.* 1982, **92**, 670.

90. J.-M. Pan, B. L. Maschhoff, U. Diebold and T. E. Madey, *J. Vac. Sci. Technol. A* 1992, **10**, 2470.

91. P. Salvador, M. L. G. Godlez and F. Mdoz, *J. Phys. Chem.* 1992*,* **96***,* 10349.

92. Q. Zhong, J. M. Vohs and D. A. Bonnell, *J. Am. Ceram. Soc.* 1993, **76**, 1137.

93. W. E. Wallace, Q. Zhong, J. Genzer, R. J. Composto and D. A. Bonnell, *J. Mater. Res.* 1993, **8**, 1629.

94. R. R. Hasiguti and E. Yagi, *Phys. Rev. B* 1994, **49**, 7251.

95. E. Yagi, R. R. Hasiguti and M. Aono, *Phys. Rev. B* 1996, **54**, 7945.

96. T. Fujino, M. Katayama, K. Inudzuka, T. Okuno, K. Oura and T. Hirao, *Appl. Phys. Lett.* 2001, **79**, 2716.

97. T. Sekiya, T. Yagisawa, N. Kamiya, D. Das Mulmi, S. Kurita, Y. Murakami and T. Kodaira, *J. Phys. Soc. Jpn.* 2004, **73**, 703.

98. T. Xia and X. Chen, *J. Mater. Chem. A*, 2013, **1**, 2983.

99. X. Chen, L. Liu, Z. Liu, M. A. Marcus, W.-C. Wang, N. A. Oyler, M. E. Grass, B. Mao, P.-A. Glans, P. Y. Yu, J. Guo and S. S. Mao, *Sci. Rep.* 2013, **3**, 1510.

100. L. Liu, P. P. Yu, X. Chen, S. S. Mao, D. Z. Shen, *Phys. Rev. Lett.* 2013, **111**, 065505.

101. C. Sun, Y. Jia, X.-H. Yang, H.-G. Yang, X. Yao, G. Q. (Max) Lu, A. Selloni and S. C. Smith, *J. Phys. Chem. C* 2011, **115**, 25590.

102. H. Lu, B. Zhao, R. Pan, J. Yao, J. Qiu, L. Luo and Y. Liu, *RSC Adv.*, 2014, **4**, 1128.

103. N. Liu, C. Schneider, D. Freitag, M. Hartmann, U. Venkatesan, J. Muller, E. Spiecker and P. Schmuki, *Nano Lett.* 2014, **14**, 3309.

104. J. Qiu, S. Li, E. Gray, H. Liu, Q.-F. Gu, C. Sun, C. Lai, H. Zhao and S. Zhang, *J. Phys. Chem. C* 2014, **118**, 8824.

105. J. Qiu, C. Lai, E. Gray, S. Li, S. Qiu, E. Strounina, C. Sun, H. Zhao and S. Zhang, *J. Mater. Chem. A* 2014, **2**, 6353.

106. W. Wang, Y. Ni, C. Lu and Z. Xu, *RSC Adv.* 2012, **2**, 8286.

107. W. Wang, C. Lu, Y. Ni, M. Su, Z. Xu, *Appl. Catal. B* 2012, **127**, 28.

108. W. Wang, Y. Ni, C. Lu and Z. Xu, *Appl. Surf. Sci.* 2014, **290**, 125.

109. T. Leshuk, S. Linley and F. Gu, *Can. J. Chem. Eng.* 2013, **91**, 799.

110. T. Leshuk, R. Parviz, P. Everett, H. Krishnakumar, R. A. Varin and F. Gu, *ACS Appl. Mater. Interfaces* 2013, **5**, 1892.

111. J. E. Rekoske and M. A. Barteau, *J. Phys. Chem. B* 1997, **101**, 1113.

112. H. Liu, H.T. Ma, X.Z. Li, W.Z. Li, M. Wu and X.H. Bao, *Chemosphere* 2003, **50**, 39.

113. X. Yu, B. Kim and Y. K. Kim, *ACS Catal.* 2013, **3**, 2479.

114. G. Li, Z. Zhang, H. Peng and K. Chen, *RSC Adv.* 2013, **3**, 11507.

115. X. Lu, G. Wang, T. Zhai, M. Yu, J. Gan, Y. Tong and Y. Li, *Nano Lett.* 2012, **12**, 1690.

116. S. Li, J. Qiu, M. Ling, F. Peng, B. Wood and S. Zhang, *ACS Appl. Mater. Interfaces* 2013, **5**, 11129.

117. C. Zhang, H. Yu, Y. Li, Y. Gao, Y. Zhao, W. Song, Z. Shao and B. Yi, *ChemSusChem* 2013, **6**, 659.

118. G. Wang, H. Wang, Y. Ling, Y. Tang, X. Yang, R. C. Fitzmorris, C. Wang, J. Z. Zhang and Y. Li, *Nano Lett.* 2011, **11**, 3026.

119. A. Naldoni, M. Allieta, S. Santangelo, M. Marelli, F. Fabbri, S. Cappelli, C. L. Bianchi, R. Psaro, and V. Dal Santo. *J. Am. Chem. Soc.* 2012, **134**, 7600.

120. C. Barzan, E. Groppo, S. Bordiga and A. Zecchina, *ACS Catal.* 2014, **4**, 986.

121. X. Jiang, Y. Zhang, J. Jiang, Y. Rong, Y. Wang, Y. Wu and C. Pan, *J. Phys. Chem. C* 2012, **116**, 22619.

122. Z. Liang, G. Zheng, W. Li, Z. W. Seh, H. Yao, K. Yan, D. Kong and Y. Cui, *ACS Nano* 2014, **8**, 5249.

123. J.-Y. Shin, J. H. Joo, D. Samuelis and J. Maier, *Chem. Mater.* 2012, **24**, 543.

124. W.-D. Zhu, C.-W. Wang, J.-B. Chen, D.-S. Li, F. Zhou and H.-L. Zhang, *Nanotechnology* 2012, **23**, 455204.

125. Z. Lu, C.-T. Yip, L. Wang, H. Huang and L. Zhou, *ChemPlusChem* 2012, **77**, 991.

126. L. Shen, E. Uchaker, X. Zhang and G. Cao, *Adv. Mater.* 2012, **24**, 6502.

127. A. Danon, K. Bhattacharyya, B. K. Vijayan, J. Lu, D. J. Sauter, K. A. Gray, P. C. Stair and E. Weitz, *ACS Catal.* 2012, **2**, 45.

128. S. Zhang, S. Zhang, B. Peng, H. Wang, H. Yu, H. Wang, F. Peng, *Electrochem. Commun.* 2014, **40**, 24.

129. L. Zeng, W. Song, M. Li, D. Zeng, C. Xie, *Appl. Catal. B* 2014, **147**, 490.

130. J. Wang, L. Shen, P. Nie, G. Xu, B. Ding, S. Fang, H. Dou and X. Zhang, *J. Mater. Chem. A* 2014, **2**, 9150.

131. S. Hoang, S. P. Berglund, N. T. Hahn, A. J. Bard and C. B. Mullins, *J. Am. Chem. Soc.* 2012, **134**, 3659.

132. H. He, K. Yang, N. Wang, F. Luo and H. Chen, *J. Appl. Phys.* 2013, **114**, 213505.

133. D. Wang, X. Zhang, P. Sun, S. Lu, L. Wang, C. Wang, Y. Liu, *Electrochim. Acta* 2014, **130**, 290.

134. Z. Zheng, B. Huang, J. Lu, Z. Wang, X. Qin, X. Zhang, Y. Dai and M.-H. Whangbo, *Chem. Commun.* 2012, **48**, 5733.

135. Y. Zhu, D. Liu and M. Meng, *Chem. Commun.* 2014, **50**, 6049.

136. S.-T. Myung, M. Kikuchi, C. S. Yoon, H. Yashiro, S.-J. Kim, Y.-K. Sun and B. Scrosati, *Energy Environ. Sci.* 2013, **6**, 2609.

137. Z. Wang, C. Yang, T. Lin, H. Yin, P. Chen, D. Wan, F. Xu, F. Huang, J. Lin, X. Xie and M. Jiang, *Adv. Funct. Mater.* 2013, **23**, 5444.

138. F. Teng, M. Li, C. Gao, G. Zhang, P. Zhang, Y. Wang, L. Chen, E. Xie, *Appl. Catal. B* 2014, **148–149**, 339.

139. Y. Yan, B. Hao, D. Wang, G. Chen, E. Markweg, A. Albrecht and P. Schaaf, *J. Mater. Chem. A* 2013, **1**, 14507.

140. Z. Wang, C. Yang, T. Lin, H. Yin, P. Chen, D. Wan, F. Xu, F. Huang, J. Lin, X. Xie and M. Jiang, *Energy Environ. Sci.* 2013, **6**, 3007.

141. H. Cui, W. Zhao, C. Yang, H. Yin, T. Lin, Y. Shan, Y. Xie, H. Gu and F. Huang, *J. Mater. Chem. A* 2014, **2**, 8612.

142. H. Yin, T. Lin, C. Yang, Z. Wang, G. Zhu, T. Xu, X. Xie, F. Huang and M. Jiang, *Chem. Eur. J.* 2013, **19**, 13313

143. G. Zhu T. Lin, X. Lu, W. Zhao, C. Yang, Z. Wang, H. Yin, Z. Liu, F. Huang and J. Lin, *J. Mater. Chem. A* 2013, **1**, 9650.

144. C. Yang, Z. Wang, T. Lin, H. Yin, X. Lu, D. Wan, T. Xu, C. Zheng, J. Lin, F. Huang, X. Xie and M. Jiang, *J. Am. Chem. Soc.* 2013, **135**, 17831.

145. T. Lin, C. Yang, Z. Wang, H. Yin, X. Lu, F. Huang, J. Lin, X. Xie and M. Jiang, *Energy Environ. Sci.* 2014, **7**, 967.

146. Z. Zhao, H. Tan, H. Zhao, Y. Lv, L.-J. Zhou, Y. Song and Z. Sun, *Chem. Commun.* 2014, **50**, 2755.

147. X. Zou, J. Liu, J. Su, F. Zuo, J. Chen and P. Feng, *Chem. Eur. J.* 2013, **19**, 2866.

148. Q. Kang, J. Cao, Y. Zhang, L. Liu, H. Xu and J. Ye, *J. Mater. Chem. A* 2013, **1**, 5766.

149. S. Tominaka, Y. Tsujimoto, Y. Matsushita and K. Yamaura, *Angew. Chem. Int. Ed.* 2011, **50**, 7418.

150. S. Tominaka, *Inorg. Chem.* 2012, **51**, 10136.

151. X. Liu, S. Gao, H. Xu, Z. Lou, W. Wang, B. Huang and Y. Dai, *Nanoscale* 2013, **5**, 1870.

152. L. R. Grabstanowicz, S. Gao, T. Li, R. M. Rickard, T. Rajh, D.-J. Liu and T. Xu, *Inorg. Chem.* 2013, **52**, 3884.

153. Z. Pei, L. Ding, H. Lin, S. Weng, Z. Zheng, Y. Hou and P. Liu, *J. Mater. Chem. A* 2013, **1**, 10099.

154. T. Kako, N. Umezawa, K. Xie and J. Ye, *J. Mater. Sci.* 2013, **48**, 108.

155. C. Xu, Y. Song, L. Lu, C. Cheng, D. Liu, X. Fang, X. Chen, X. Zhu and D. Li *Nanoscale Res. Lett.* 2013, **8**, 391.

156. Z. Zhang, M. N. Hedhili, H. Zhu and P. Wang, *Phys. Chem. Chem. Phys.* 2013, **15**, 15637.

157. H. Li, Z. Chen, C. K. Tsang, Z. Li, X. Ran, C. Lee, B. Nie, L. Zheng, T. Hung, J. Lu, B. Pan and Y. Y. Li, *J. Mater. Chem. A* 2014, **2**, 229.

158. H. Zhou and Y. Zhang, *J. Phys. Chem. C* 2014, **118**, 5626.

159. L. Zheng, H. Cheng, F. Liang, S. Shu, C. K. Tsang, H. Li, S.-T. Lee and Y. Y. Li, *J. Phys. Chem. C* 2012, **116**, 5509.

160. J. Dong, J. Han, Y. Liu, A. Nakajima, S. Matsushita, S. Wei and W. Gao, *ACS Appl. Mater. Interfaces* 2014, **6**, 1385.

161. T. Xia , C. Zhang, N. A. Oyler and X. Chen, Ad*v. Mater.* 2013, **25**, 6905.

162. T. Xia , C. Zhang, N. A. Oyler and X. Chen, J. *Mater. Res.* 2014, **29,** 2198.

163. M. M. Khader, F. M. N. Kheiri, B. E. Elanadouli and B. G. Ateya, *J. Phys. Chem.* 1993, **97**, 6074.

164. H. Haerudin, S. Bertel and R. Kramer, *J. Chem. Soc., Faraday Trans.* 1998, **94**, 1481.

165. Pesci, F. M.; Wang, G. M.; Klug, D. R.; Li, Y.; Cowan, A. J. *J. Phys. Chem. C* 2013, **117**, 25837.

166. Z. Pei, L. Ding, H. Lin, S. Weng, Z. Zheng, Y. Hou and P. Liu, *J. Mater. Chem. A* 2013, **1**, 10099.

167. M. M. Khan, S. A. Ansari, D. Pradhan, M. O. Ansari, D. H. Han, J. Lee and M. H. Cho, *J. Mater. Chem. A* 2014, **2**, 637.

168. J. Lu, Y. Dai, H. Jin and B. Huang, *Phys. Chem. Chem. Phys.* 2011, **13**, 18063.

169. H. Pan, Y.-W. Zhang, V. B. Shenoy and H. Gao, *J. Phys. Chem. C* 2011, **115**, 12224.

170. U. Aschauer and A. Selloni, *Phys. Chem. Chem. Phys.* 2012, **14**, 16595.

171. P. Raghunath, W. F. Huang and M. C. Lin, *J. Chem. Phys.* 2013, **138**, 154705.

172. M. Sotoudeh, S. J. Hashemifar, M. Abbasnejad and M. R. Mohammadizadeh, *AIP Adv.* 2014, **4**, 027129.

173. H.-X. Deng, S.-S. Li, J. Li and S.-H. Wei, *Phys. Rev.* 2012, **85**, 195328.

174. L. Liu, Q. Liu, Y. Zheng, Z. Wang, C. Pan and W. Xiao, *J. Phys. Chem. C* 2014, **118**, 3471.

175. L. A. Harris and R. Schumacher, *J. Electrochem. Soc.* **1980**, *127*, 1186.

176. A. Heller, Y. Degani, D. W. Johnson and P. K. Gallagher, *J. Phys. Chem.* 1987, **91**, 5987.

177. A. Gallo, M. Marelli, R. Psaro, V. Gombac, T. Montini, P. Fornasiero, R. Pievo and V. Dal Santo, *Green Chem.* 2012, **14**, 330.

178. A. Gallo, T. Montini, M. Marelli, A. Minguzzi, V. Gombac, R. Psaro, P. Fornasiero and V. Dal Santo, *ChemSusChem* 2012, **5**, 1800.

179. W. Wang, C.-H. Lu, Y.-R. Ni, J.-B. Song and Z.-Z. Xu, *Catal. Commun.* **2012**, *22*, 19.

180. X. Pan and Y.-J. Xu, *Appl. Catal. A: General* 2013, **459**, 34.

181. X. Pan and Y.-J. Xu, *ACS Appl. Mater. Interfaces* 2014, **6**, 1879.

182. M. Kong, Y. Li, X. Chen, T. Tian, P. Fang, F. Zheng and X. Zhao, *J. Am. Chem. Soc.* 2011, **133**, 16414.

183. J. N. Schrauben, R. Hayoun, C. N. Valdez, M. Braten, L. Fridley and J. M. Mayer, *Science* 2012, **336**, 1298.

184. L. Liu and Y. Li, *Aerosol Air Quality Res.* 2014, **14**, 453.

185. P. Szymanski and M. A. El-Sayed, *Theor. Chem. Acc.* 2012, **131**, 1202.

186. H. Park, Y. Park, W. Kim and W. Choi, *J. Photochem. Photobiol. C* 2013, **15**, 1.

187. T. Xia, Y. Zhang, J. Murowchick and X. Chen, *Catal. Today* 2014, **225**, 2.

188. T. Xia, W. Zhang, J. Murowchick, G. Liu and X. Chen, *Nano Lett.* 2013, **13**, 5289.

189. T. Xia, W. Zhang, J. Murowchick, G. Liu and X. Chen, *Adv. Energy Mater.* 2013, **3**, 1516.

190. Z. Wang, Y. Zhang, T. Xia, J. Murowchick, G. Liu and X. Chen, *Energy Technol.* 2014, **2**, 376.

191. T. Xia, W. Zhang, Z. Wang, Y. Zhang, X. Song, J. Murowchick, V. Battaglia, G. Liu and X. Chen, *Nano Energy*, 2014, **6**, 109.

Table 1. Properties of black TiO_2 nanomaterials

Starting TiO_2	Reaction conditions	Color	Core/shell structure	Ti^{3+}	Oxygen vacancies	Ti-OH	Ti-H	Shift of valence band	Electrical conductivity	Ref. no.
Rutile single crystal	600 °C in H_2	Blue	N/S	N/S	√	N/S	N/S	N/S	↑	82,83
Rutile single crystal	600 – 900 °C in H_2, 2.5 – 15 min	Blue to opaque	N/S	√	√	N/S	N/S	N/S	↑	84
Rutile single crystal	600 – 800 °C in H_2, 2.5 – 15 min	N/S	N/S	√	√	N/S	N/S	N/S	↑	85
Anatase nanocrystals	200 °C in 20 bar H_2, 5 d	Black	√	×	×	↑	√	√	N/S	75
Anatase (001) nanocrystals	450 °C in 7 MPa H_2, 24 h	Blue	×	N/S	N/S	√	N/S	N/S	N/S	101
Anatase (101) nanocrystals	450 °C in 7 MPa H_2, 24 h	Black	×	N/S	N/S	√	N/S	N/S	N/S	101
Anatase-rutile P25 nanocrystals	RT in 35 bar H_2, 20 d	Black	√	√	N/S	↓	N/S	N/S	N/S	102
Anatase nanotubes	500 °C in H_2/Ar flow, 1 h	Black	×	√	√	√	N/S	N/S	↑	103
Anatase nanotubes	500 °C in 20 bar H_2, 1 h	Blue	×	√	√	√	N/S	N/S	↑	103
Rutile nanocrystals	450 °C in 40 bar H_2, 1 h	Blue to gray	N/S	√	√	N/S	N/S	N/S	↑	104
Anatase (001) nanosheets	200 – 500 °C in 10 bar H_2, 2 h	Dark blue, gray	N/S	√	√	√	√	×	N/S	106-108
Anatase	200 °C in 300	Black	N/S	N/S	N/S	N/S	N/S	N/S	N/S	109

nanocrystals	psi H_2, 5 d or 400 –500 °C, 24 – 102 h									
SiO_2/TiO_2 core/shell nanocrystals	250 – 450 °C in 20 bar H_2, 24 h	Black	N/S	×	√	√	√	×	N/S	110
Anatase nanoparticles	20 – 700 °C in H_2 flow, 2 h	N/S	N/S	√	√	N/S	N/S	N/S	N/S	112
Anatase (001) nanosheets	500 – 700 °C in H_2 flow, 0.5 – 10 h	Blue to gray	N/S	√	√	N/S	√	N/S	N/S	113
Anatase microspheres	400 °C in ambient pressure H_2, 1 h	Gray	N/S	√	√	N/S	N/S	N/S	↑	114
Anatase nanotubes	300 – 600 °C in ambient pressure H_2, 1 h	N/S	N/S	√	√	↑	N/S	N/S	↑	115
Anatase nanotubes	450 °C in ambient pressure H_2, 2 h	N/S	N/S	×	√	↑	N/S	N/S	↑	116
Anatase nanotubes	200 – 600 °C in ambient pressure H_2, 1 h	N/S	N/S	×	√	↑	N/S	N/S	↑	117
Rutile nanowires	200 – 550 °C in ambient pressure H_2, 3 h	Yellow, green to black	N/S	×	√	↑	×	×	↑	118
Amorphous nanoparticles	500 °C in H_2 flow, 1 h	Black	√	√	√	↑	×	√	N/S	119
Anatase-rutile P25	500 °C in 200 mbar H_2, 1 h	Blue	×	√	N/S	N/S	×	N/S	N/S	120

nanocrystals										
Anatase-rutile P25 nanocrystals	400 °C in ambient pressure H_2, 10 h	Gray	√	√	√	N/S	N/S	N/S	N/S	121
Anatase-rutile opals	500 °C in 80 Torr H_2, 10 h	Darker	N/S	√	√	N/S	N/S	N/S	↑	122
Anatase nanocrystals	450 °C in 5% H_2-95% Ar flow, 1-7 h	Yellow to dark yellow	N/S	N/S	√	N/S	N/S	N/S	↑	123
Anatase nanotubes	450 °C in H_2 (8 sccum)-Ar (10 sccm) flow, 5 h	N/S	N/S	√	√	N/S	N/S	N/S	↑	124
Anatase nanotubes	450 °C in 5% H_2-95% Ar flow, 1 h	Black	×	√	√	↓	N/S	×	↑	125
Titanate nanowires	500 - 700 °C in 5% H_2 v/v Ar, 1.5 h	N/S	√	√	N/S	N/S	N/S	N/S	↑	126
Titanate nanotubes	350 °C in 5% H_2 in Ar, 3 h	Blue, black	×	×	N/S	N/S	N/S	N/S	N/S	127
Rutile nanorods	350 °C in H_2 (20 sccm) Ar (80 sccm) flow, 3 h	Gray	N/S	√	√	N/S	N/S	N/S	↑	128
Anatase nanoparticles	300 °C in H_2/Ar flow, 2 h	N/S	√	√	√	√	N/S	N/S	N/S	129
Anatase-RGO nanoparticles	450 °C in 5% H_2/95% Ar flow, 4 h	N/S	N/S	√	N/S	N/S	N/S	N/S	↑	130

Anatase nanoparticles	350 °C in 6% H_2/94% N_2 flow, 2 h	Yellow	N/S	N/S	N/S	N/S	N/S	N/S	↑	132
Rutile nanorods	400 °C in 10% H_2/90% N_2, 30 min	Gray	√	N/S	√	N/S	N/S	N/S	↑	133
Anatase nanowire microspheres	500 °C in 5% H_2 in N_2 flow (300 sccm), 4 h	Dark brown	√	√	N/S	↓	√	N/S	N/S	1341
Anatase-rutile P25/Pt	200 – 700 °C in 8% H_2 in N_2, 4 h	×	√	×	√	↑	×	N/S	N/S	135
Amorphous gel	200, 300, 400 – 600 °C in Ar 5 h	Dark yellow, green, black	N/S	√	√	N/S	N/S	N/S	↑	136
Anatase-rutile P25 nanoparticles	500 °C in H_2 plasma (200 W) 4 – 8 h	Black	√	×	√	↑	√	×	N/S	137
Anatase nanotubes, nanosheets	350 – 500 °C in H_2 plasma 3 h	Black	√	√	√	N/S	√	N/S	N/S	138
Anatase nanoparticles	390 °C in H_2 plasma (3000 W), 50 sccm H_2 flow, 3 h	Black	√	√	√	√	×	N/S	↑	139
Anatase nanoparticles	300 – 500 °C by Al (800 °C) reduction 6 – 20 h	Black	√	√	√	N/S	N/S	×	N/S	140

Anatase nanotubes	500 °C by Al (850 °C) reduction 4 h	Black	√	√	√	N/S	N/S	√	↑	141
Anatase nanowires	200 – 900 °C by Al (800 °C) reduction 4 h	Gray	√	√	√	N/S	N/S	N/S	N/S	142
Brookite nanoparticles	300 – 600 °C by Al (800 °C) reduction 4 h	Black	√	√	√	N/S	N/S	√	N/S	143
Anatase, rutile S-doped nanoparticles	500 °C by Al (800 °C) reduction 4 h	Black	√	√	√	N/S	N/S	√	N/S	144
Anatase-rutile P25 H, N, S, I-doped nanoparticles	500 °C by Al (800 °C) reduction 4 h	Black	√	√	√	N/S	N/S	N/S	N/S	145
Rutile nanorods	180 °C $TiCl_3$ (1 mL, 15-20%) in IPA with Zn (0.5 – 2.5 mmol) 6 h	Gray to dark blue	×	√	√	N/S	N/S	N/S	N/S	146
Amorphous precursor	180 °C Imidazole, HCl 6 h	Gray	N/S	×	√	N/S	N/S	N/S	N/S	147
Anatase nanotubes	RT 0.1 M $NaBH_4$ 10 – 60 min	Gray	N/S	√	√	×	×	√	N/S	148
Rutile nanoparticles	180 °C CaH_2 10 – 15 d	Black	×	√	√	√	N/S	N/S	↑	149, 150
TiH_2 powders	180 °C H_2O_2	Blue	N/S	√	√	×	×	N/S	N/S	151

	(25wt%) 20 -27 h									
TiH_2 powders	RT H_2O_2 23 h + 180 °C 16 h + 630 °C Ar 3 h	Black	×	√	×	×	×	N/S	N/S	152
TiO powders	160 °C in HCl (3 M) 24 h	Gray	×	√	√	N/S	N/S	N/S	N/S	153
Ti_2O_3 powders	550 – 900 °C 3 h	Grayish green, yellow	×	√	√	N/S	N/S	N/S	N/S	154
Anatase nanotubes	5 V in 0.5 M Na_2SO_4 5 – 40 s	Blue black	N/S	N/S	√	N/S	N/S	N/S	N/S	155
Anatase nanotubes	0.4 V in 1 M Na_2SO_4 30 min	Dark blue	N/S	√	N/S	N/S	N/S	N/S	N/S	156
Anatase nanotubes	40 V in EG 0.27 wt% NH_4F 200 s	Black	N/S	×	√	√	×	√	↑	157
Anatase nanotubes	20 V in EG 2 h	Black	N/S	√	√	√	×	N/S	↑	158
Anatase nanotubes	1.65 V5 – 30 s	Black	N/S	√	N/S	N/S	N/S	N/S	N/S	159
Anatase nanotubes	450 °C 1 h	Black	√	×	√	√	N/S	N/S	N/S	160

Notes: N/S: not studied; √: yes; ×: no; ↑: increase; ↓: decrease; RT: room temperature; RGO: reduced graphene oxide; EG: ethylene glycol; IPA: isopropanol.